Shared gene targets of the ATF4 and p53 transcriptional networks

Gabriele Baniulyte[1], Serene A. Durham[1], Lauren E. Merchant[1], Morgan A. Sammons[1,a]

[1]*Department of Biological Sciences and The RNA Institute*, University at Albany, State University of New York, Albany, NY, USA

[a] Corresponding author: masammons@albany.edu

Abstract

The master tumor suppressor p53 regulates multiple cell fate decisions, like cell cycle arrest and apoptosis, via transcriptional control of a broad gene network. Dysfunction in the p53 network is common in cancer, often through mutations that inactivate p53 or other members of the pathway. Induction of tumor-specific cell death by restoration of p53 activity without off-target effects has gained significant interest in the field. In this study, we explore the gene regulatory mechanisms underlying a putative anti-cancer strategy involving stimulation of the p53-independent Integrated Stress Response (ISR). Our data demonstrate the p53 and ISR pathways converge to independently regulate common metabolic and pro-apoptotic genes. We investigated the architecture of multiple gene regulatory elements bound by p53 and the ISR effector ATF4 controlling this shared regulation. We identified additional key transcription factors that control basal and stress-induced regulation of these shared p53 and ATF4 target genes. Thus, our results provide significant new molecular and genetic insight into gene regulatory networks and transcription factors that are the target of numerous antitumor therapies.

Keywords: *cis-regulation, genomics, enhancers, transcription, transcription factors, p53, ATF4*.

Introduction

The global rewiring of cellular anabolic and catabolic processes that result from homeostatic changes include dynamic control of RNA and protein synthesis and turnover (Vihervaara et al., 2018; Advani and Ivanov, 2019). The DNA damage-inducible transcription factor, p53, directly activates transcription of a broad range of target genes involved in DNA repair, cell cycle arrest, and apoptosis. The well-described tumor suppressor function of p53 primarily relies on transcriptional activation of these target genes and their ability to mitigate the consequences of damaged DNA. Nearly half of human malignancies harbor mutations in p53 that facilitate and promote metastasis, tumorigenesis, and resistance to apoptosis (Zhu et al., 2015; Mantovani et al., 2019). These mutations generally lead to loss of DNA binding and an inability to transactivate canonical anti-proliferative p53 target genes (Bykov et al., 2018). Genotoxic chemotherapeutics, like doxorubicin and etoposide, are clinically relevant activators of wild-type p53, but the potential risk of resistance and secondary malignancies due to increased mutational burden remains a significant concern (Aziz et al., 2011). Given the powerful tumor suppression abilities of p53, restoration of the p53-regulated transcriptome without inducing additional DNA damage represents an intriguing approach for development of anticancer strategies and therapeutics.

Non-genotoxic, small molecule activation of the p53 pathway has been proposed as a potential solution. The first general approach involves small-molecule targeting of mutant p53 to restore its wild-type function or prevent dominant-negative/gain-of-function activities (Yu et al., 2012; Chowdhury et al., 2014; Zhang et al., 2015; Bykov et al., 2018). A second approach uses compounds like the MDM2 inhibitor nutlin-3A to activate wild-type p53 in a non-genotoxic fashion, although early clinical trials suggest these approaches have limited efficacy when used alone (Andreeff et al., 2016; Kocik et al., 2019; Montesinos et al., 2020). A third approach involves bypassing p53 altogether via compounds that activate key anti-proliferative p53 targets in p53-deficient tumors (Hernandez Borrero et al., 2021; Tian et al., 2021). These compounds engage the Integrated Stress Response (ISR) network which is an effector of anti-proliferative and cell death gene expression programs. Interestingly, simultaneous ISR activation and MDM2 inhibition led to

51 significant cell death and tumor regression not observed when the approaches were used individually
52 (Andrysik et al., 2022), suggesting these pathways may work synergistically. These new ISR-stimulating
53 approaches may be broadly applicable, as wild-type p53, p53-deficient, and p53 missense mutation-
54 containing tumors could all be targeted. Thus, further exploration into the genetic and biochemical basis
55 underlying this shared synergy between the p53 and ISR gene regulatory networks is needed for the design
56 of more efficacious therapeutics with known mechanisms of action.
57
58 Here, we examine shared gene targets and regulatory strategies of two distinct stress-dependent pathways,
59 the p53 gene regulatory network (GRN) and the ATF4-dependent Integrated Stress Response (ISR)
60 pathway. We identify an enhancer element required for p53-dependent induction of *ATF3* in response to
61 DNA damage, however, is not directly required for transcription of *ATF3* under ISR activating conditions.
62 ISR-dependent induction of *ATF3* requires ATF4 via binding and regulation of the *ATF3* promoter. We
63 identified a second regulatory strategy whereby ATF4 and p53 target a shared enhancer to control
64 *GADD45A,* another common gene target. Our data suggest that the p53 and ISR pathways have shared gene
65 targets and begin to unravel the DNA encoding and TF requirements for engagement of *cis*-regulatory
66 elements driving these behaviors.
67
68 **Materials & Methods**
69
70 ***Cell Culture and Treatments***
71 The human colorectal cancer cell lines, HCT116 TP53$^{+/+}$ and HCT116 TP53$^{-/-}$, were cultured in McCoy's
72 5A Media (Corning, #10-050-CV) supplemented with 10% Fetal Bovine Serum (FBS) (Corning, #35-016-
73 CV) and 1% Penicillin-Streptomycin (Gibco, #15240-062). Human mammary epithelial cells, MCF10A
74 TP53$^{+/+}$ and MCF10A TP53$^{-/-}$ (Sigma-Aldrich) were cultured in 1:1 Dulbecco's Modified Eagle Medium:
75 Ham's F-12 (Gibco, #11330-032) supplemented with 5% horse serum (Gibco, #16050-122), 20 ng/ml
76 epidermal growth factor (Peprotech, #AF-100-15), 0.5 ng/ml hydrocortisone (Sigma, #H-0888), 100 ng/ml

77 cholera toxin (Sigma, #C-8052), 10 µg/ml insulin (Sigma, #I-1882), and 1% Penicillin-Streptomycin
78 (Gibco, #15240-062). The human near haploid cell line, HAP1 parental and HAP1 *ATF4*$^{-}$ cells (Horizon
79 Genomics, HZGHC007380c010), were cultured in Iscove's Modified Dulbecco's Medium (Gibco, #12440-
80 053) supplemented with 10% Fetal Bovine Serum (FBS) (Corning, #35-016-CV) and 1% Penicillin-
81 Streptomycin (Gibco, #15240-062). All cell lines were cultured at 37°C and 5% CO_2 in a water-jacketed
82 incubator.
83 For cell line treatments, cells were cultured for times indicated in each experimental figure/legend with
84 either 5 µM nutlin-3A (Millipore Sigma, #45-SML0580) to stabilize p53 activation, 100 µM etoposide
85 (Thermo Scientific, #J63651.MC), 2 µM tunicamycin (Thermo Scientific, #J62217.MA) or 2 mM histidinol
86 (Acros Organics, #AC228831000). All drugs were freshly resuspended in DMSO and DMSO-only controls
87 were added at equal volumes to each drug treatment.
88
89 ***Luciferase plasmid cloning and expression assays***
90 Relevant plasmids and primers with cloning design are listed in Table S1. All cloning was done using
91 NEBuilder (NEB, #E2621S). NanoLuciferase reporter plasmids were constructed using GADD45a_pHG
92 plasmid as a backbone (kind gift from A. Fornace). pGB7 is the wild-type equivalent plasmid used
93 throughout this study and includes *GADD45A* region chr1:67682954-67690203 (hg38) with translationally
94 fused *nLuc*. pGB7 also engineered to have PacI, Esp3I and MunI sites to facilitate removal of the 5' UTR
95 and/or promoter region.
96
97 Luciferase assays were carried out using Nano-Glo® Dual-Luciferase® Reporter Assay System (Promega
98 #1620) following manufacturer's recommendations. NanoLuciferase or firefly luciferase values were
99 normalized to constitutively expressed firefly luciferase (fLuc), or nanoLuciferase (nLuc) levels that were
100 generated by co-transfected pGL4.53 or pNL1.1 (Promega, #E5011, #N1441) plasmids, respectively.
101
102 ***dCas9-KRAB gRNA cloning***

103 All primers used to generate gRNAs are listed in Table S1. To generate a transfer plasmid for each dCas9-
104 KRAB genomic target region, forward and reverse primer pairs were annealed and then cloned into the
105 BsmBI restriction site in the pLV hU6-sgRNA hUbC-dCas9-KRAB-T2a-Puro vector (gift from C.
106 Gersbach, Addgene #71236). HCT116 cell lines constitutively expressing dCas9-KRAB and appropriate
107 targeting gRNA were generated as described in (Thakore et al., 2015). All treatments are described Material
108 and Methods above and in the figure legend.
109
110 ***Lentivirus production, purification and transduction***
111 Lentiviral particles were packaged using HEK293FT cells seeded at a density of 250,000 cells per well in
112 6-well culture plates. In brief, 1 µg of pLKO.1-Puro TRC plasmid containing either non-targeting control
113 shRNA (5'-CAACAAGATGAAGAGCACCAA-3') or ATF4-targeted shRNA (5'-
114 GCCTAGGTCTCTTAGATGATT-3') was combined with 1 µg of packaging plasmids psPAX2 and
115 pMD2.G, mixed at a molar ratio of 2:1. The plasmid mix was diluted in jetPRIME buffer (Polyplus
116 Transfection, 89129-924) and transfection reagent, following the manufacturer's protocol. pMD2.G and
117 psPAX2 were gifts from Didier Trono (Addgene plasmid # 12259, #12260). Lentiviral supernatants were
118 collected at 24 and 48 h post-transfection, supplemented with 8 µg/ml Polybrene, filtered through 0.45-µm
119 nitrocellulose filters, and stored at −80 °C. Cells were transduced with lentivirus and were selected for viral
120 infection via addition of 2 µg/mL of puromycin for 72 hours.
121
122 **Quantitative Real Time PCR (RT-qPCR)**
123 Total RNA was isolated (Quick RNA, Zymo, #R1055) with on-column DNase I digestion for 30 minutes.
124 Single-stranded cDNA was generated (High Capacity cDNA Reverse Transcription Kit, ABI #4368814)
125 and qPCR was performed using the relative standard curve method and iTaq Universal SYBR Green
126 Supermix reagents (BioRad). All RT-qPCR primers are presented in Table S1.
127
128 ***Western Blotting***

129 Total protein was isolated using a custom RIPA buffer (50mM Tris-HCl[pH 7.4], 150mM NaCl, 1% NP-
130 40, 0.5% sodium deoxycholate, 0.1% SDS) supplemented with protease/phosphatase inhibitors (Pierce,
131 78442). Protein concentration was measured using the BCA approach (Pierce, 23227), and equal protein
132 concentrations were analyzed using the ProteinSimple® Wes platform with the 12–230 kDa Wes
133 Separation Module containing 8 × 25 capillary cartridges per manufacturer's instructions. Specific
134 antibodies used were: anti-p53 (clone DO-1, BD Bioscience #554293), anti-ATF3 (Abcam, #AB207434),
135 anti-ATF4 (Cell Signaling, #D4B8), anti-GADPDH (Cell Signaling, #5174S).
136
137 ***CUT&RUN***
138 $1.5x10^6$ cells per CUT&RUN reaction and three biological replicates per condition were prepared for batch
139 processing using the Epichyper CUTANA™ CUT&RUN protocol v1.9 and reagents (Epicypher, #14-
140 1048). Briefly, cells bound to Concanavalin A beads were incubated overnight with 0.5 µg of anti-ATF4
141 antibody or non-specific rabbit IgG. DNA fragments were purified using phenol/chloroform extraction and
142 20 ng of purified DNA was used to construct an Illumina-compatible sequencing library (Liu, 2019)
143 optimized for CUT&RUN-sized DNA fragments and NEBNext Ultra II DNA Library reagents (NEB
144 #E7660). Library concentrations were quantified (NEBNext Library Quant Kit, E7630), pooled at
145 equimolar concentrations, and sequenced on the Illumina NextSeq 2000 at the University at Albany Center
146 for Functional Genomics.
147
148 ***CUT&RUN and ChIP-seq Data Analysis***
149 Raw paired-end sequencing reads for CUT&RUN were aligned to the hg38 human genome reference using
150 hisat2 (Kim et al., 2019) with the following options (-X 700 -I 10 --no-spliced-alignment). Regions of
151 significant ATF4 enrichment (relative to IgG control signal) were identified using *macs2* (Zhang et al.,
152 2008). ChIP-seq reads (Andrysik et al., 2017) for HCT116 input (GSM2296270), p53 ChIP-seq under
153 DMSO-treatment (GSM2296271), and p53 ChIP-seq under nutlin-3A-treatment (GSM2296272) were
154 downloaded from Gene Expression Omnibus and aligned to the hg38 human genome reference using hisat2.

155 BigWig files for visualization were produced via deepTools (Ramírez et al., 2016). Gene set enrichment
156 for ATF4 CUT&RUN peaks was performed using ChIP-Enrich based on distance to the nearest
157 Transcriptional Start Site (TSS) (Welch et al., 2014).
158
159 ***RNA Sequencing***
160 Cells were treated with either DMSO, nutlin-3A, etoposide, tunicamycin, or histidinol as described above
161 in a six-well plate for 6h and total RNA was isolated (Quick RNA miniprep, Zymo, #R1055). PolyA+ RNA
162 was purified using Dynabeads Oligo $(dt)_{25}$ (Invitrogen, #61012) and fragmented at 94°C for 15 min.
163 Fragmented RNA was used as the template for double-stranded cDNA production which was then used to
164 construct an Illumina-compatible sequencing library (NEBNext Ultra II Directional RNA Library, NEB
165 E7760). Libraries were then pooled for sequencing on an Illumina NextSeq 2000 at the University at Albany
166 Center for Functional Genomics or on an Illumina Hiseq 2000 at Azenta/GeneWiz. Transcript abundance
167 from the ENSEMBL hg38 genome assembly (v.104) was quantified using *kallisto* (quant -b 100) (Bray et
168 al., 2016). Resulting transcript counts (TPM) were imported and processed via tximport (Soneson et al.,
169 2015) and differential expression was quantified using DESeq2 (Love et al., 2014). Pathway enrichment
170 analyses for differentially expressed genes were performed using enrichr (Chen et al., 2013; Kuleshov et
171 al., 2016; Xie et al., 2021). Upstream regulator analysis on differentially-expressed genes was performed
172 using the Causal Inference Engine (Farahmand et al., 2019) querying the TRRUST database (Han et al.,
173 2018) using Fisher's Exact Test settings and the STRINGdb (Szklarczyk et al., 2022) with the Quaternary
174 Scoring statistic (Fakhry et al., 2016).
175
176 ***STARRSeq enhancer mutagenesis screen***
177 STARRSeq library preparation was done following a published protocol (Neumayr et al., 2019) with minor
178 modifications as described here. To simplify STARRSeq library preparation, hSTARR-seq_ORI vector
179 (Addgene #99296) (Muerdter et al., 2018) was modified by adding partial Illumina P5 and P7 adaptor
180 sequence before AgeI and after SalI restriction sites, respectively, yielding plasmid pGB118. Mutagenesis

181 library was constructed as a 250 nt of *GADD45A* intronic enhancer region (chr1:67686701-67686950) with
182 a 'N' mixed base or a deletion at every position and 25 nt pGB118 matching overhangs on the 5' and 3'
183 ends. The library was ordered as an oligo pool (oPool, IDT). oPool library was amplified for 10 cycles with
184 primers SL1947 + SL1948 and cloned into pGB118 cut with AgeI and SalI using NEBuilder (NEB,
185 #E2621S). 18 million HCT116 $TP53^{+/+}$ or $TP53^{-/-}$ cells were transfected with 10 µg STARRSeq
186 mutagenesis plasmid library using JetPrime Transfection Reagent (Polyplus #101000046) following
187 manufacturer's recommendations. 5h after transfection, the media was replaced with fresh media
188 supplemented with 0.001% DMSO, 5 µM nutlin-3A or 2 µM tunicamycin. RNA was extracted 6h post-
189 treatment. Processed RNA and plasmid DNA libraries were sequenced on Illumina NextSeq 2000
190 instrument at the University at Albany Center for Functional Genomics as 2x150 paired-reads. R1 and R2
191 reads were first merged using bbmerge tool from BBMap (Bushnell et al., 2017). Merged reads were then
192 collected and counted using a strict string pattern matching the expected library sequences. Relative
193 expression was calculated as an RNA/DNA ratio.
194
195 **Results**
196
197 ***ATF3 is induced by the Integrated Stress Response (ISR) in a p53-independent manner***
198 Activating Transcription Factor 3 (*ATF3)* is an immediate-early response gene in the cellular adaptive-
199 response network. *ATF3* mRNA is upregulated in response to cellular stress including both DNA damage
200 and endoplasmic reticulum (ER) stress (Hai et al., 1999; Hashimoto et al., 2002; Jiang et al., 2004; Hai,
201 2006; Lu et al., 2006). Recent reports suggest activation of the ISR leads to induction of p53 target genes,
202 including *ATF3*, but the specific transcription factor requirements for this behavior have not been fully
203 characterized. Thus, we investigated whether p53 was required for ATF3 induction under both DNA
204 damage and ISR conditions. We confirmed *ATF3* mRNA expression is induced by both p53 and ISR
205 pathways in HCT116 *TP53*+/+ (p53 WT) or *TP53*-/- (p53 null) colorectal carcinoma cells. We used two
206 independent means to activate the p53 and ISR pathways. Etoposide activates p53 via induction of DNA

207 double strand breaks (DSBs) (van Maanen et al., 1988; Shieh et al., 1997). Nutlin-3A specifically inhibits
208 the negative p53 regulator, MDM2, leading to highly specific activation of p53 in a non-genotoxic manner
209 (Vassilev et al., 2004). In vertebrates, the ISR is activated by ER stress, nutrient and heme deprivation, and
210 viral infection, amongst others (Taniuchi et al., 2016). Therefore, we treated our HCT116 cell lines with
211 tunicamycin, an inhibitor of N-linked glycosylation which induces ER stress via accumulation of unfolded
212 proteins (Ding et al., 2007), or histidinol, which initiates the amino acid response (AAR) via depletion of
213 histidine (Fu and Kilberg, 2013).
214
215 We first confirmed the specificity of these treatments via examination of p53 protein abundance and
216 expression of canonical p53 and ISR target genes *CDKN1A/*p21 and the asparagine synthetase *ASNS*,
217 respectively (el-Deiry et al., 1993; Szak et al., 2001; Siu et al., 2002). p53 protein (Fig. 1B) and
218 *CDKN1A/*p21 mRNA (Fig. 1D) expression increased in response to both etoposide and nutlin-3A in a p53-
219 dependent manner but not after ISR activation by tunicamycin or histidinol. Both ER stress and AA
220 starvation led to *ASNS* induction in a p53-independent manner (Fig. 1E). Neither nutlin-3A nor etoposide
221 treatments altered *ASNS* mRNA abundance in either genetic background, suggesting the ISR is not activated
222 after DNA DSB induction. Taken together, these results suggest tunicamycin- and histidinol-mediated
223 induction of the ISR in HCT116 cells does not require p53 activity (Fig. 1D, E). Although the induction of
224 *ASNS* mRNA under ISR stimulating conditions relative to DMSO vehicle control was not dependent on
225 p53, we note that the total abundance of *ASNS* mRNA is slightly reduced in HCT116 p53 null cell line (Fig.
226 1E).
227
228 *ATF3* mRNA and protein levels increased under both p53 and ISR stimulating treatments in HCT116 WT
229 cells (Fig. 1A, C). p53 is required for induction of *ATF3* mRNA in response to nutlin-3A and etoposide,
230 whereas ATF3 protein is still induced in response to etoposide in the absence of p53. Total ATF3 protein
231 abundance is considerably lower in HCT116 p53 null cells relative to HCT116 WT suggesting that p53
232 activity is required for basal, but not induced, *ATF3* expression. Importantly, *ATF3* mRNA and protein

233 induction is p53-independent under ISR stimulating conditions (Fig 1A, C). Coupled with the lack of p53
234 stabilization and *CDKN1A/p21* induction, these data suggest that upregulation of *ATF3* in response to ISR
235 does not require p53.
236
237 ***ATF4 and p53 independently regulate expression of ATF3***
238 Our results suggest that both p53 and the ISR regulate *ATF3* transcription in a parallel, potentially redundant
239 fashion. ATF4, a member of the basic region-leucine zipper (bZIP) TF superfamily, is one of the main
240 transcriptional effectors of the ISR (Chen et al., 1996; Han et al., 2013). Prior work suggests ATF4 regulates
241 expression of *ATF3* in other cellular contexts, therefore we tested whether ATF4 controls p53-independent
242 induction of *ATF3* mRNA expression in response to ER stress and AA starvation (Pan et al., 2007; Kilberg
243 et al., 2009; Fu and Kilberg, 2013). We first characterized the activity of *ATF4* in response to ISR-activating
244 stimuli in our HCT116 p53 WT and p53 null cells to confirm ISR-dependent *ATF4* expression. As expected,
245 *ATF4* mRNA and protein levels increase in response to both ER stress (via tunicamycin treatment) and AA
246 starvation (via histidinol treatment), whereas *ATF4* mRNA and protein expression were unaffected in
247 response to p53 stabilization (via nutlin-3A treatment) or DNA damage (via etoposide treatment) (Fig. 2A,
248 D).
249
250 To determine the role of ATF4 in regulating *ATF3* induction downstream of ISR activation, we created
251 HCT116 p53 WT and p53 null cells expressing either a non-targeting control shRNA or *ATF4*-targeted
252 shRNA. *ATF4* mRNA and protein are substantially reduced in *ATF4* shRNA-expressing cells compared to
253 non-targeting control shRNA (Fig. 2B, E), as was the ATF4 target *ASNS,* demonstrating the effectiveness
254 of shRNA in ablating ATF4 (Fig. 2I). *ATF3* induction in response to etoposide was unaffected by *ATF4*
255 depletion (Fig. 2G). Conversely, *ATF4* knockdown significantly reduced *ATF3* mRNA induction in
256 response to ER stress, suggesting a direct role for ATF4 activity in mediating ISR-dependent *ATF3*
257 expression (Fig. 2G). We extended our analysis to isogenic *ATF4*+ (HAP1 parental) and *ATF4*- (HAP1
258 ATF4KO) haploid leukemia cell lines. *ATF4* mRNA and protein levels were not induced in response to ER

259 stress in HAP1 *ATF4*- cell line (Fig. 2C, F). Undetectable ATF4 protein in the *ATF4*- cell line results from
260 a 2 bp insertion in exon 3 of *ATF4* that truncates the protein, including the DNA-binding domain. Lack of
261 *ATF4* mRNA induction during ER stress in *ATF4*- cells suggests that ATF4 protein might be involved in
262 *ATF4* autoregulation, however there is currently no evidence suggesting direct regulation (Dey et al., 2010).
263 Inactivation of ATF4 led to a complete ablation of both *ASNS* and *ATF3* mRNA induction in response to
264 ER stress, confirming *ATF3* induction in response to ISR is ATF4-dependent (Fig. 2H, J). These results
265 demonstrate that ATF4 is the main effector of ISR-mediated *ATF3* induction and that p53 mediates *ATF3*
266 transcription after DNA damage.
267
268 ***ATF4 and p53 occupy distinct regulatory regions in the ATF3 gene locus***
269 Our results demonstrate a genetic dependence for p53-mediated activation of *ATF3* transcription under
270 DNA damage conditions, and a functionally distinct, ATF4-dependent pathway that regulates *ATF3*
271 transcription during the ISR. To understand whether direct ATF4 binding to regulatory regions controls
272 *ATF3*, we generated novel cleavage under targets & release under nuclease (CUT&RUN) (Skene and
273 Henikoff, 2017) data for ATF4 in HCT116 cells treated with either DMSO (control), p53-activating
274 (etoposide), or ISR-stimulating agents (tunicamycin or histidinol) using either an ATF4-specific antibody
275 or a non-specific IgG control. We generated high-confidence, ISR-activated ATF4 binding events by
276 considering called peaks from 5 out of 6 experiments from cells treated with either tunicamycin or histidinol
277 (Fig. S1A-C). The rationale for this peak filtering strategy is to restrict further analysis of universal ISR-
278 dependent ATF4 binding events, while also accounting for biological or technical variability in replicates.
279 In support of this approach, we observe 7,723 ATF4 binding events shared across five out of six
280 experimental conditions, with 5,093 (65%) existing across all observations. These 7,723 peaks were then
281 examined for expected features of ATF4 binding, including specificity during ISR stimulation and
282 enrichment of predicted ATF4 DNA binding motifs.
283

284 Known motif enrichment analysis revealed the ATF4 motif as enriched in high-confidence peaks, followed
285 by enrichment of the known heterodimer partner, C/EBP homologous protein (CHOP) (Fig. 3A). Similar
286 enrichment of a motif most closely matching the known ATF4 motif was observed using *de novo*
287 enrichment strategies (Fig. 3B). Enrichment of CUT&RUN tags was highly specific for tunicamycin and
288 histidinol treatment conditions compared to either vehicle DMSO or etoposide conditions (Fig. 3C). To
289 provide context into the functional relevance of ATF4 binding, our CUT&RUN analysis reveals a
290 significant, ISR-specific enrichment of ATF4 at the *ASNS* promoter (Fig. S1D), confirming previous reports
291 that AA starvation-induced *ASNS* expression is mediated via ATF4 interaction with the promoter (Chen et
292 al., 2004), We also assessed whether the ATF4 high-confidence binding was associated with genes in the
293 ISR or other known pathways. We used ChIP-Enrich to perform gene pathway enrichment analyses on
294 genes nearest to either our ATF4 binding events or previously identified p53 binding events from nutlin-
295 3A-treated HCT116 cells (Welch et al., 2014; Andrysik et al., 2017). Genes in the Unfolded Protein
296 Response and aminoacyl-tRNA biosynthesis pathways are highly enriched gene sets associated with ATF4
297 binding when querying the mSigDB, KEGG, and REACTOME databases (Fig. 3E-G), in support of our
298 ATF4 CUT&RUN data representing functional binding events. p53 binding events are associated with
299 genes involved in apoptosis, DNA repair, and the response to stress, as expected (Fig. 3E-G). Interestingly,
300 these analyses revealed both ATF4 and p53 binding events are significantly associated with genes in the
301 canonical p53 pathway, including *ATF3* (Fig. 3E-F). Taken together, these data suggest that our high-
302 confidence, ISR-dependent ATF4 peaks likely represent true ATF4 genomic binding events and further
303 suggest a link between the ATF4-dependent ISR and the p53 network.
304
305 Given the genetic evidence that *ATF3* is regulated by both p53 and ATF4 and our genome-wide ATF4
306 binding experiments, we next surveyed the *ATF3* gene locus to identify putative ATF4 and p53 binding
307 events that might directly regulate *ATF3* transcription. We observe ATF4 binding within a previously
308 identified promoter regulating ISR-dependent *ATF3* transcription (Fu and Kilberg, 2013) in response to
309 both ER stress and amino acid deprivation, but not during the DDR or in DMSO control conditions (Fig.

310 3D). p53, on the other hand, binds to a DNAse Hypersensitive Site (DHS) approximately 13 kb upstream
311 (p53-bound DHS) from the ATF4-bound *ATF3* promoter. ATF4 also occupies a spatially distinct DHS
312 15kb upstream (ATF4-bound DHS) from the *ATF3* TSS in an ISR-dependent fashion. These novel genomic
313 binding datasets for ATF4 further suggest a direct role for ATF4 in regulation of ISR-dependent *ATF3* and
314 confirm the ATF4-independence of *ATF3* transcription downstream of DNA damage.
315
316 ***Analysis of the regulatory elements controlling stress dependent ATF3 expression***
317 Biochemical analyses and genetic loss-of-function experiments confirm p53 and ATF4 independently
318 regulate expression of *ATF3* (Figs. 1-3). To determine if the distinct p53 or ATF4-bound DHS contribute
319 directly to transcription of *ATF3* in response to stress, we tested their ability to activate transcription of a
320 luciferase reporter gene via a minimal promoter (minP). The upstream ATF4-bound DHS does not act as
321 an enhancer, as there was no significant difference in transcription compared to the negative control (minP
322 only), under any conditions and cellular contexts tested (Fig. 4A). The p53-bound DHS drove substantial
323 transcriptional activity under basal conditions with a significant increase in activity upon nutlin-3A
324 treatment. Basal and p53-induced activity were significantly reduced when the putative p53 binding motif
325 was mutated or when assayed in HCT116 p53 null cell lines. Loss of p53 does not completely ablate basal
326 transcription, suggesting other transcription factors likely contribute to unstimulated *ATF3* activity.
327 However, no additional transcriptional activation by the p53-bound DHS was observed in response to
328 tunicamycin (Fig. 4A). Taken together, these data suggest that the p53-bound DHS likely regulates *ATF3*
329 transcription under basal and conditions that stabilize p53, and that the adjacent ATF4-bound DHS likely
330 does not facilitate ISR-mediated *ATF3* transcription.
331
332 Prior work suggests ATF4 regulates *ATF3* via interaction with two canonical ATF/CREB family motifs
333 within the *ATF3* promoter in hepatocarcinoma (HepG2) cells (Fu and Kilberg, 2013). This regulation
334 depends on both a CRE site (nt −90/−82, TTACGTCAG) and a CARE site (nt −21/−13, TGATGXAAX)
335 within the *ATF3* gene promoter (−104/+36) (Weidenfeld-Baranboim et al., 2009; Hai et al., 2010). We thus

336 assessed whether ATF4 regulates *ATF3* via interaction with these elements, as ISR-induced ATF4 binding
337 to an upstream DHS had no effect on *ATF3* transcription (Fig. 4A). We thus tested activity of luciferase
338 reporters driven by the −104/+36 promoter fragment of the *ATF3* gene - containing both the CARE and
339 CRE sequences (WT ATF3 promoter), as well as constructs containing mutations in one (CARE and CRE)
340 or both (CARE/CRE) of these sites, in control and ATF4-deficient HAP1 cell lines. Consistent with prior
341 reports, both ER stress (tunicamycin) and AA starvation (histidinol) treatments led to increased
342 transcription driven by the WT *ATF3* promoter in an ATF4-dependent manner (Fig. 4B). Mutation of the
343 CARE and CRE sites, both capable of supporting ATF4 binding, showed significantly and substantially
344 reduced ability to drive both basal and ISR-induced transcription. Our data are consistent with prior
345 observations that the CARE site is required for amino acid starvation-induced activity, but is dispensable
346 for ER stress-induced transcription (Pan et al., 2007; Fu and Kilberg, 2013). Similar to our results for the
347 upstream p53-bound DHS, these data suggest that multiple transcription factors in addition to p53 and
348 ATF4 are likely involved in the basal and stress-dependent regulation of *ATF3*, consistent with models
349 whereby multiple transcription factors work in a context-dependent and combinatorial manner to drive
350 transcription (Smith et al., 2013; Chaudhari and Cohen, 2018; Zeitlinger, 2020; Choi et al., 2021; Kim et
351 al., 2021). Our data using genetic depletion strategies, biochemical binding assays, and testing putative *cis*-
352 regulatory element activity using reporter assays provide evidence for a model whereby *ATF3* transcription
353 in response to DNA damage and the ISR occurs through distinct transcription factors binding to distinct
354 regulatory elements.
355
356 ***ISR-mediated induction of ATF3 does not require the upstream enhancer bound by p53***
357 ATF4 and p53 likely independently regulate expression of *ATF3* by occupying distinct putative regulatory
358 regions in a stress-dependent manner (Figs. 2G, 3D, 4A-B). To further characterize the mutual
359 independence of p53 and ATF4 and to demonstrate whether these binding events control *ATF3* transcription
360 *in vivo*, we utilized a CRISPR interference (CRISPRi) system to block effector protein binding at these
361 elements (Gilbert et al., 2013; Qi et al., 2013). We chose the dCas9-KRAB CRISPRi system which fuses a

362 catalytically inactive *Streptococcus pyogenes* Cas9 with a KRAB transcriptional repressor domain
363 (Margolin et al., 1994). dCas9-KRAB targeting to *cis*-regulatory elements is an effective strategy for
364 blocking effector protein binding and inhibiting regulatory elements and linked gene expression (Thakore
365 et al., 2015; Yeo et al., 2018; Catizone et al., 2020). We first targeted dCas9-KRAB to the *ATF3* promoter
366 as proof of principle, since repression of a gene promoter should inhibit transcription initiated from that
367 element. Targeting of dCas9-KRAB to the *ATF3* promoter, approximately 100 bp upstream of the TSS
368 significantly reduced *ATF3* mRNA levels (Fig. 4D). *ATF3* mRNA levels were unaffected when targeting
369 dCas9-KRAB to the off-target p53-bound *FGF2* enhancer (chr4:122,798,358, *hg38*) or a region 13kb
370 upstream (5') of the putative *ATF3* enhancer (Fig. 4D). A similar lack of repression was observed when
371 dCas9-KRAB is targeted to a region equidistant (6kb) from both the putative *ATF3* enhancer and promoter
372 (3' downstream relative to the enhancer) (Fig. 4D). This repression when targeting the promoter was
373 observed under basal (DMSO), DNA damage, and ER stress conditions, demonstrating the effectiveness of
374 the CRISPRi system. Targeting dCas9-KRAB to the p53-bound enhancer significantly reduced *ATF3*
375 mRNA levels in response to basal and etoposide-treated conditions when compared to all non-targeting
376 controls (Fig. 4D). Targeting of dCas9-KRAB to any of the three control locations did not significantly
377 alter either basal or DNA damage-induced *ATF3* expression (Fig. 4D). Canonical ISR and p53 gene targets
378 *ASNS* and *CDKN1A/*p21 were unaffected by targeting dCas9-KRAB to the p53-bound enhancer or control
379 regions (Fig. 4E-F). Induction of *ATF3* mRNA in response to tunicamycin-induced ER stress was not
380 affected when targeting the p53-bound enhancer (Fig. 4D). These results indicate the p53-bound enhancer
381 is important for both basal and p53-mediated activation of *ATF3*, but is not directly required for ER stress-
382 mediated induction of *ATF3*.
383
384 ***Global transcriptome analysis identifies common gene regulatory targets of the p53 and Integrated Stress***
385 ***Response***
386

387 Our data demonstrate that the DNA damage response (DDR, via p53) and the Integrated Stress Response
388 (ISR, via ATF4) independently activate transcription of *ATF3* through at least two gene regulatory
389 elements. We sought to determine if this parallel stress-dependent gene activation by the p53 and ISR
390 pathways may be more widespread. We thus performed polyA+ RNA-seq on HCT116 p53 WT and p53
391 null cells after 6 hours of treatment with p53 or ISR-activating stimuli: DMSO (vehicle), 5 μM nutlin-
392 3A,100 μM etoposide, 2 μM tunicamycin, or 2 mM histidinol. Three biological replicates were analyzed
393 for each treatment condition via transcript counting (*kallisto*, 100 bootstraps) (Bray et al., 2016) and
394 differential gene expression analysis (*deseq2)* (Love et al., 2014). We confirmed that each treatment elicited
395 an expected transcriptional response using gene ontology analysis of significantly upregulated (Fig. S2A-
396 D) or downregulated (Fig. S2E-H) genes when compared to DMSO control (Chen et al., 2013; Kim et al.,
397 2019; Xie et al., 2021). Treatment with either nutlin-3A or etoposide led to significant upregulation of genes
398 (184 and 1,394, respectively) consistent with a functional p53 response, including those related to the
399 cellular response to DNA damage (Fig. S2A-B). Treatment with tunicamycin led to upregulation of 2,138
400 genes consistent with ER stress and transcriptional regulation (Fig. S2C) and downregulation of 2,131 genes
401 involved in translation and ribosome biogenesis (Fig. S2G). Similar ontology groups were enriched in
402 differentially regulated genes after treatment with histidinol (Fig. S2D,H), although we note treatment
403 specific enrichment of ER stress-associated genes after tunicamycin treatment and metabolic regulation
404 after histidinol addition. Nearly 50% of the genes upregulated in response to either tunicamycin or histidinol
405 have an ATF4 binding event within 10kB of their transcriptional start site (Fig. 5B), further supporting that
406 these genes are likely regulated via ATF4 and the ISR. Taken together, these broad analyses of gene
407 regulation via standard gene ontology methods demonstrate that each chemical treatment recapitulates
408 expected cellular responses to specific cell stress conditions.
409
410 We next wanted to identify additional genes that might be co-regulated by ATF4 and p53 and examine
411 potential upstream regulators for both gene networks. We first used the Causal Inference Engine approach
412 to identify potential upstream regulators of the differentially expressed genes identified in our RNA-seq

413 analysis from the TRRUST network database (Han et al., 2018; Farahmand et al., 2019). ATF4 is predicted
414 to be a significant regulator for both tunicamycin and histidinol-induced genes, but not etoposide in both
415 WT and p53 null cell lines (Fig. 5C, S3A). ATF6 and XBP1, other transcription factors activated by ER
416 stress, are also putative regulators of tunicamycin-induced genes, in agreement with their expected role in
417 mediating ER stress (Pakos-Zebrucka et al., 2016). Interestingly, this approach also predicts p53 is a likely
418 regulator of ISR-mediated gene expression in both WT and p53 null cells and across both the TRRUST and
419 STRING networks (Fig. 5C, S3A-C). These data, combined with our extensive genetic and biochemical
420 analyses of *ATF3* regulation, suggest additional genes may be co-regulated by these two core cellular stress
421 responses via similar mechanisms to *ATF3.*
422
423 We therefore established parameters to define genes that can be independently activated by p53 and the
424 ISR. We reasoned that these genes would be i) significantly upregulated in response to both p53- and ISR-
425 activating stimuli in HCT116 p53 WT cells relative to DMSO, ii) p53-dependent in response to nutlin-3A
426 treatment, a stimulus that specifically activates and stabilizes p53 (Fig. S2I), and iii) significantly
427 upregulated in the absence of p53 in response to ISR-activating treatments, tunicamycin and histidinol. The
428 inclusion of nutlin-3A-mediated regulation limits our gene set to those genes regulated by p53 specifically,
429 as opposed to via DNA damage-dependent, but p53-independent mechanisms, as we have previously
430 observed (Catizone et al., 2020). Ultimately, these criteria yielded 26 genes upregulated in response to p53
431 activation, ER stress, and AA starvation (Fig. 5A). As expected, *ATF3* was in this gene set upregulated in
432 response to all four treatment conditions relative to DMSO, providing support for selection criteria and the
433 quality of the data set (Fig. 5E-F). Gene ontology analysis of these 26 genes suggests shared involvement
434 in apoptotic signaling pathways and transcription by RNA polymerase II. We also observed regulation of
435 the mitogen-activated protein kinase (MAPK) signaling cascade, which integrates and amplify signals from
436 diverse stimuli (Zhang and Dong, 2007; Chavel et al., 2010) (Fig. 5D). Pathway analysis on shared
437 downregulated genes reveal common function in protein synthesis, potentially reflecting a switch from an
438 anabolic to catabolic state, consistent with prior reports of broad translational control by these pathways

439 (Fig. 5D) (Loayza-Puch et al., 2013; Zaccara et al., 2014; Andrysik et al., 2017; Tameire et al., 2019; Tian
440 et al., 2021).
441
442 We next analyzed the behavior of commonly upregulated genes in HCT116 p53 null cells to determine
443 whether induction is truly p53-dependent or independent in response to ISR-inducing stimuli. Heirarchical
444 clustering (one minus Pearson correlation with complete linkage) revealed two distinct groups of these
445 genes (Group 1 and Group 2). 11 of the 26 commonly upregulated genes behave similarly to *ATF3* (Figs.
446 5E-F) and cluster together in Group 1. The remaining genes (Group 2) show some dependence on p53 for
447 full activation downstream of the ISR. p53 protein levels are not stabilized in response to ISR-activating
448 stimuli (Fig. 1B) and we observe no evidence that canonical p53 targets like *CDKN1A*/p21 respond to ISR-
449 activating stimuli (Fig. 1D), suggesting that this partial dependence on p53 is likely due to indirect activity
450 of p53 in regulating other activators within the ISR. Consistent with this, we note diminished ATF4 protein
451 in the absence of p53 in basal and ISR-induced conditions (Fig. 2A). While additional work is required to
452 determine the causal relationship, if any, between loss of p53, reduced ATF4 protein abundance, and the
453 effect on ISR-dependent gene expression, our data suggest that p53 and ATF4-dependent transcriptional
454 control mechanisms are likely to be functionally independent.
455
456 Lastly, we validated the p53 and ATF4-dependence of a set of common genes using a battery of cell lines
457 and genotypes. We examined p53-dependence for three candidate genes regulated similarly to *ATF3*:
458 *GADD45A* (Zhan et al., 1994; Ebert et al., 2019), *SESN2* (Budanov and Karin, 2008; Garaeva et al., 2016),
459 and *GDF15* (Osada et al., 2007; Li et al., 2021). We tested the behavior of these three genes in response to
460 etoposide or tunicamycin treatment in p53 WT and p53 null HCT116 (Fig. 6A-D) and MCF10A mammary
461 epithelial lines (Fig. 6E-H). Each gene was induced by both treatments and etoposide-mediated induction
462 required an intact p53 response. Conversely, p53 was not required for induction in response to tunicamycin,
463 consistent with the parallel nature of the p53 and ATF4-dependent transcriptional networks. These data in
464 MCF10A cell lines also demonstrate that this behavior is not limited to colon carcinoma cell lines. We then

465 assessed ATF4-dependence of these genes in either HAP1 parental or *ATF4*- cell lines and found that *ATF4*
466 activity is required for tunicamycin induction (Fig. 6I-L). Nutlin-3A treatment fails to induce expression of
467 *ATF3, GADD45A, SESN2,* and *GDF15* likely due to the loss-of-function *TP53* S215G allele (Moder et al.,
468 2017) in these cell lines. The absence of p53 and the presence of a functional ISR further suggest the
469 functional independence of these pathways. Our data thus identify a set of "dual response" genes
470 independently regulated by p53 or ATF4 in response to specific stress conditions.
471
472 ***GADD45A gene-derived reporter system for assessing DDR and ISR enhancers***
473 Our data demonstrate p53 activates *ATF3* transcription through a distal enhancer, whereas we confirmed
474 observations that ATF4 regulates transcription via the *ATF3* proximal promoter. We sought to determine
475 whether any additional "dual response" genes have *cis*-regulatory strategies like *ATF3*. We focused on
476 *GADD45A* which was reported to contain a p53-bound enhancer within the 3rd intron (Zhan et al., 1998;
477 Daino et al., 2006). Our CUT&RUN analysis suggests ATF4 also binds to this putative enhancer (Fig. 7A).
478 We thus tested whether p53 and ATF4 binding to this element controls *GADD45A* transcription under p53
479 or ISR activating conditions, respectively, utilizing a newly constructed luciferase reporter system (Fig.
480 7B). We reasoned that (1) *GADD45A* is relatively small (~3 kb) and is convenient for plasmid-based genetic
481 manipulations, and that (2) this reporter might be more relevant for stress-dependent promoter-enhancer
482 interaction studies as a near native genetic context, including enhancer:promoter distance and location, is
483 maintained. We tested four versions of the "native" *GADD45A-nLuc* system, creating transcriptional or
484 translational fusion constructs either with or without a degron tag (hPEST) (Fig. S4). Luciferase activity
485 was detectable in all four versions under basal conditions, and constructs lacking the degron tag were
486 inducible by p53 (nutlin-3A) and ISR stimulating (tunicamycin) conditions (Fig. S4B), consistent with our
487 results measuring native GADD45A mRNA expression (Fig. 6B). All subsequent experiments utilize the
488 *GADD45A-nLuc* translational fusion lacking the degron tag due to the highest signal-to-noise ratio in our
489 initial tests (Fig. S4B).
490

491 To confirm the putative *cis*-element in the 3rd intron is essential for *GADD45A-nLuc* reporter activity, we
492 characterized luciferase activity in response to mutation or deletion of nucleotides predicted to be critical
493 for binding of p53 and/or ATF4. The intronic enhancer has conserved p53RE and AP1 motifs that were
494 previously reported to be required for ionizing radiation induced *GADD45A* expression (Chin et al., 1997;
495 Daino et al., 2006; Smeenk et al., 2008). We additionally identified one canonical ATF4 motif
496 (TGATGAAA, minus strand, Fig. 7C) using the JASPAR database (Castro-Mondragon et al., 2022).
497 ATF/AP1 transcription family motifs are highly similar (Bejjani et al., 2019) (Fig. 7C, S5) and ATF4 can
498 form heterodimers with other AP1 family members (Hai and Curran, 1991; Podust et al., 2001; Mann et al.,
499 2013), thus we included mutants of both motifs to identify the true ISR response element in the *GADD45A*
500 enhancer. The wild-type *GADD45A-nLuc* reporter system responds to the p53 and ISR pathways like the
501 native *GADD45A* gene (Fig. 7D). An intact p53RE motif was required for maximal enhancer-driven
502 transcription under basal conditions and consistent with prior work (Daino et al., 2006). Disrupting this
503 motif (Fig. 7C) resulted in low expression levels like deletion of the entire 250bp DHS region suggesting
504 that p53 is a major regulator of basal *GADD45A* transcription. Nutlin-3A-mediated transcription was
505 completely dependent on the p53RE motif, whereas ATF4 and AP1 motifs were dispensable (Fig. 7D).
506 Disrupting the predicted ATF4 motif had no effect on basal or tunicamycin-induced expression whereas
507 disrupting the AP1 motif decreased basal activity and tunicamycin-mediated induction (Fig. 7D),
508 suggesting that ISR pathway is regulated, at least partially, through the AP1 motif. Both the p53 and AP1
509 motifs appear to play key roles in the basal expression of *GADD45A,* but the motifs appear to be
510 functionally distinct in response to p53 and ISR-stimulating conditions. We also included combinatorial
511 motif mutants to investigate whether transcription factors binding to these motifs are activating
512 independently. If the predicted ATF4 motif was not functional, one would expect that the double
513 inactivation of p53RE and ATF4 motif would behave as p53RE mutant and would still be inducible by
514 tunicamycin. In contrast, we observed lack of tunicamycin-mediated induction when the reporter had
515 combined p53RE and ATF4 motif mutations. In fact, all constructs that included ATF4 and/or AP1
516 mutations in different combinations were not inducible by tunicamycin (Fig. 7D). It is possible that the

517 ATF4 motif is not required under normal conditions but could act redundantly in the absence of the
518 preferred AP1 motif.
519
520 ***Nucleotide-level characterization of the GADD45A enhancer reveals critical regulatory sequences***
521 Enhancers are generally regulated by multiple transcription factors (TFs) acting positively or negatively
522 depending on context (Kim and Wysocka, 2023). p53 binding primarily positively regulates enhancer
523 activity, although the extent to which additional transcription factors are required for p53-dependent *trans*-
524 activation remains an open question (Verfaillie et al., 2016; Catizone et al., 2020). Our observations suggest
525 the AP1 motif adjacent to the p53RE in the *GADD45A* intronic enhancer is required for maximal
526 transcriptional output but is not required for p53-dependent induction. Conversely, this AP1 binding site is
527 strictly required for tunicamycin-induced enhancer activity, suggesting that the regulatory potential of this
528 enhancer is context-dependent. The *GADD45A* intron 3 enhancer is predicted to encode at least 10 distinct
529 TF motifs (JASPAR 2022 (Castro-Mondragon et al., 2022)). To identify additional TF motifs regulating
530 context-dependent enhancer activity, we measured basal and stimulus-dependent enhancer activity using
531 STARRSeq (self-transcribing active regulatory region sequencing) (Muerdter et al., 2018). We performed
532 nucleotide-resolution saturating mutagenesis with all possible substitutions or single nucleotide deletion at
533 every position within the 250 bp enhancer (Fig. 8A). First, this library was transiently transfected into the
534 HCT116 wild-type and p53 null cell lines to assess p53 dependence. Cells were also treated with DMSO,
535 nutlin-3A, or tunicamycin to measure p53 or ISR-mediated activation of the *GADD45A* enhancer reporter
536 library (Fig. 8B, S5). Overall, most single-nucleotide substitutions and deletions had little or no effect on
537 basal or drug-induced activity (Fig. 8B, S5).
538
539 Consistent with our *GADD45A*-full gene reporter assays (Fig. 7D), nucleotide substitutions and deletions
540 at consensus motif positions with high predicted importance for p53 binding severely diminished enhancer
541 activity in wild-type HCT116 cell line (Fig. 8C), with near perfect concordance to the canonical p53RE
542 motif. Changes in the critical half-site positions of p53RE (nucleotide positions 78-81 and 88-91)

543 consistently disrupted enhancer-driven transcription. Most nucleotide substitutions in the 6 bp spacer
544 between the half-sites had minimal or no effect on enhancer activity (nucleotide positions 83-87). For
545 example, T>A or T>C substitutions at the first position of the spacer are well-tolerated, but in agreement
546 with known p53 binding preferences, T>G substitution reduced enhancer activity (Fig. 8C). T>C (position
547 3 of the spacer) and G>A (position 6) substitutions increased enhancer activity, again mirroring the shift
548 closer to consensus p53 binding preferences. Conversely, all single nucleotide deletions disrupted enhancer
549 activity, illustrating the well-studied importance of spacing between half-sites for p53 binding and activity
550 (el-Deiry et al., 1992) (Fig. 8C). Comparison of nucleotide substitutions between WT and p53 null
551 conditions suggests most of the substitutions with altered activity require an intact p53 response, except for
552 A85G and A86G substitutions. Although these nucleotide changes are predicted to be more like the
553 consensus sequence than wild type RE and display increased enhancer activity, they also show increased
554 activity in p53 null cells, suggesting these substitutions may result in a *de novo* activating TF motif or
555 disruption of a repressive TF element. Overall, loss-of-function substitutions in the p53RE did not display
556 reduced enhancer activity in p53 null cells, as the genetic loss of p53 is expected to be epistatic with
557 mutation of the p53RE (Fig. 8B). Nucleotide-resolution mutagenesis of the well-defined p53RE suggests
558 that our STARRseq assay is suitable for high-throughput mutagenesis and identification of additional
559 factors important for stress-dependent *GADD45A* enhancer.
560
561 We identified the AP1(FOS:JUN) site downstream of the p53RE, and not the predicted ATF4 upstream
562 element, to be important for both basal- and tunicamycin-induced enhancer activity using traditional
563 reporter gene assays (Fig. 7D). Disruption of the upstream ATF4 element in the saturating mutagenesis
564 STARRseq assay had little to no effect on enhancer activity, whereas we observed a marked decrease in
565 enhancer activity when the AP1 motif was disrupted in either WT or p53 null cell line (Fig. 8C, S5). The
566 loss of activity in response to AP1 motif substitutions in p53 null lines further suggests combinatorial and
567 additive roles of these two elements in driving basal enhancer activity. Specifiic substitutions to the AP1
568 (FOS:JUN) motif demonstrates a clear dependence for known AP1 family binding preferences on enhancer

activity. C>G/T substitutions at position 131 have increased activity, presumably representing a shift closer to the consensus AP1 motif (Fig. 8C). The most sensitive positions to nucleotide substitutions were the two palindromic half-sites ('TG' and 'CA') and nucleotide deletions predicted to disrupt spacing between those half-sites (Fig. 8C).

Our STARRSeq assay for the *GADD45A* intron 3 enhancer revealed multiple nucleotide substitutions with increased or decreased activity. Individual nucleotide changes can disrupt TF motifs important for wild-type *GADD45A* enhancer activity but could also represent varied activity due to *de novo* creation of TF binding sites or experimental noise. Therefore, to identify other true positive TF motifs, we focused our analysis on contiguous 6+ nucleotide regions that display altered activity when (1) multiple substitutions and deletions at the same position have similar effects, (2) changes in several adjacent positions have similar effect, and (3) motif mutations have negative effect on the expression and thus are potentially bound by activators. Using such criteria, we identified 3 other regions that may positively regulate *GADD45A* enhancer activity. Each of these regions overlap a specific predicted TF motif, ETV6, AP1/BACH1 or GLIS3/POU6F (Fig. S5). AP1 and BACH1 are part of the broader bZIP family of DNA binding proteins and have highly similar motif preferences. Consistent with the p53RE and the AP1 (FOS:JUN) sites, nucleotide substitutions at positions predicted to be important for either AP1 or BACH1 binding display reduced enhancer activity (Fig. 8C). These effects are observed in both WT and p53 null cell lines, suggesting this motif contributes to basal activity in a p53-independent context. An A>C substitution at position 181 strongly increases enhancer activity, likely due to C adhering more closely to the predicted consensus binding motif for both AP1 and BACH1 dimers. Nucleotide deletions at any position reduced enhancer activity, whereas we observed a position-specific effect of substitutions mirroring consensus nucleotide preferences. Our saturating mutagenesis approach validates the critical role of the previously characterized p53 and AP1 binding sites in the positive regulation of the *GADD45A* enhancer, and revealed putative, novel TF motifs that may contribute to basal or induced enhancer activity.

595 ***Validation of the STARRseq-defined effects of nucleotide substitutions within the GADD45A enhancer***
596 ***via a native-context reporter assay activity***
597 To assess whether nucleotide substitutions in newly identified *GADD45A* enhancer motifs would have the
598 same effect in a native gene context, we tested a series of 'upregulating' and 'downregulating' substitutions
599 in our *GADD45A-nLuc* reporter system (Fig. 9). All *GADD45A-nLuc* enhancer mutants were transiently
600 transfected into HCT116 wild-type and p53 null and treated with DMSO, nutlin-3A and tunicamycin. The
601 AP1/BACH1(A181C) substitution moves this motif closer to the consensus sequence and is expected to
602 improve binding and subsequent activation of *GADD45A*, whereas G177A would likely have the opposite
603 effect. Indeed, using the native reporter system demonstrates that these substitutions behave as predicted
604 from the MPRA-based approach (Fig. 8C, 9C). We next assessed how substitutions in the overlapping
605 GLIS3 and POU6F2 motifs (Fig. S5) affect activity in the more native context. All nucleotide substitutions
606 led to increased activity in the MPRA, suggesting these motifs and their bound factors may act to repress
607 *GADD45A* transcription. In the native reporter system, substitutions in this overlapping GLIS3/POU6F
608 motif increased enhancer activity (Fig. 9C), further suggesting that this sequence restrains activity of the
609 *GADD45A* enhancer.
610
611 Results from native reporter gene assays measuring the activity of nucleotide substitutions in the putative
612 ETV6 motif located between the p53 and AP1 motifs were more nuanced (Fig. 9C). ETV6 is an ETS-family
613 transcription factor and most frequently acts as a repressor (Lopez et al., 1999). The ETV6 A113G
614 substitution, which led to consistently increased activity in the MPRA (Fig. S5), displayed increased nutlin-
615 3A/p53-induced activity, but did not affect expression under basal or tunicamycin-treated conditions. The
616 A112T substitution, predicted to reduce enhancer activity, surprisingly displayed higher levels of nutlin-
617 3A-induced activity in HCT116 WT p53 using the native reporter system. Interestingly, both the ETV6
618 A112T and A113G substitutions led to diminished enhancer activity across all treatment conditions in
619 HCT116 p53 null. These data suggest a potential context-dependence of the ETV6 motif in regulation of

620 *GADD45A* enhancer activity, with motif disruptions leading to varied effects depending on the presence of
621 p53.
622
623 **Discussion**
624 In this study, we present a comparative analysis of gene regulatory strategies for two fundamental cell stress
625 responses. We demonstrate the p53 gene regulatory network and the ATF4-driven Integrated Stress
626 Response, although generally controlling distinct genes, converge on a set of common transcriptional
627 targets related to metabolic control and apoptosis. Our study provides direct evidence that these targets
628 require p53 during the DNA damage response, but not during the ISR. Conversely, ATF4 is required during
629 the ISR and is dispensable under p53-activating conditions. The genetic dependence parallels the well-
630 studied, stress-evoked stabilization of p53 and translation of ATF4 (Kastan et al., 1991; Vattem and Wek,
631 2004), which is further supported by observations that neither p53 nor ATF4 levels increase after activation
632 of the other pathway (Fig. 1B, 2A, D). Importantly, these data are consistent with recent work demonstrating
633 targeted ISR induction activates specific p53 gene targets in p53-deficient cells (Hernandez Borrero et al.,
634 2021; Tian et al., 2021). Similarly, chemical inhibition of the phosphatase PPM1D leads to increased ATF4
635 activity which synergized with p53 to amplify expression of some p53 target genes and increased cell death
636 (Andrysik et al., 2022). These data point towards therapeutic strategies broadly applicable across cancers
637 regardless of *TP53* genetic status. Combined treatment with non-genotoxic activators of p53 (like MDM2
638 inhibitors) and chemical induction of the ISR pushes cells towards an apoptotic/cell death fate, which could
639 overcome the reported limitations of MDM2 inhibition alone (Aziz et al., 2011). Small molecules restoring
640 p53 function in p53-deficient tumors are being developed and their efficacy may be bolstered by combined
641 ISR activation. These approaches are especially attractive given the non-genotoxic nature and the relatively
642 large number of experimental and approved compounds that activate p53 or the ISR.
643
644 Both the p53-dependent and the ATF4-driven ISR gene networks are antiproliferative, either through
645 induction of apoptosis or cell cycle control. p53 canonically mediates cell cycle control through

646 *CDKN1A/*p21 and other targets, like *CCNG1* (Jensen, 2003). The p53 network appears to be "redundant",
647 where loss of a single antiproliferative strategy does not appreciably affect tumor suppressor function.
648 These shared genes may represent an additional layer of redundancy to tumor suppression by p53 through
649 metabolic control. At least four of the shared p53 and ATF4 targets (*DDIT4, GADD34, SESN2,* and *GDF15)*
650 are antiproliferative via inhibition of mTOR signaling (Budanov and Karin, 2008; Gambardella et al., 2020;
651 Lockhart et al., 2020; Aguilar-Recarte et al., 2021; Coronel et al., 2022). *ATF3* also coordinates cell cycle
652 progression through serine, nucleotide, and glucose metabolic control (Ku and Cheng, 2020; Di
653 Marcantonio et al., 2021). These genes, thus, may represent a "core" repurposed by various cell stress
654 response pathways for anti-proliferative effects through the central energy regulator mTOR. Thus,
655 investigations into stress-dependent regulation of these targets by other transcription factors controlling
656 hypoxia (HIF1α), heat shock (HSF1), inflammation (IRF/STAT), xenobiotics (AHR), and infection (NF-
657 kB), may be warranted.
658
659 Our genetic dissection of *ATF3* and *GADD45A* provides mechanistic detail into independent regulation by
660 both p53 and ATF4. *ATF3* induction after stress is mediated by two spatially distinct and mutually
661 independent regulatory elements, each bound by either p53 or ATF4. While our data suggest that basal
662 *ATF3* expression is reduced when either element is perturbed, stress-mediated induction appears wholly
663 dependent on the specific stress-activated transcription factor and its unique bound element. In contrast,
664 stress dependent *GADD45A* induction is controlled by a single enhancer element bound by both p53 and
665 ATF4. STARRSeq-based saturating mutagenesis of this *GADD45A* enhancer provided nucleotide-level
666 resolution of DNA elements that control enhancer activity. Consistent with our genetic, biochemical, and
667 reporter gene analyses, this assay demonstrated nucleotide substitutions at positions predicted to be critical
668 for binding by either p53 or ATF4 most significantly impacted enhancer activity and *GADD45A* expression.
669 This is true for predicted loss-of-function nucleotide substitutions, but also substitutions that are predicted
670 to improve transcription factor binding (Fig. 8C). These data suggest that MPRA-style assays like
671 STARRseq are suitable for examining the impact of sequence differences in p53-bound elements resulting

672 from natural or disease-associated human variation (Fig. S5). This impact has not been comprehensively
673 explored, but certain gain-of-function variants with pro-tumorigenic activity have been reported (Menendez
674 et al., 2007; Zeron-Medina et al., 2013). We also identified and validated three additional transcription
675 factor binding motifs directly impacting enhancer activity. Sequence-based motif prediction methods
676 identify numerous putative transcription factor motifs within the *GADD45A* enhancer that did not alter
677 enhancer activity in this context. Enhancers have well-defined cell lineage-dependent activity based on the
678 specific combination of transcription factors that may be present (Zeitlinger, 2020; Kim et al., 2021), thus,
679 we cannot rule out that these predicted motifs may be functional in other settings. Thus, a combination of
680 unbiased saturating mutagenesis screening across diverse cell types and sequence-based motif analyses may
681 help to refine and improve the ability to predict functional elements within regulatory elements.
682
683 Our results examining p53 and ATF4-mediated induction of *GADD45A* provide new insight into the
684 complex interplay between multiple transcription factors at stress-dependent enhancers. The p53RE is
685 critical for nutlin-3A-induced expression of *GADD45A,* whereas other motifs were dispensable, including
686 the AP1 site critical for ATF4-mediated expression. These motifs are also unnecessary for ATF4-dependent
687 induction. Our observations mirror prior studies demonstrating p53-induced enhancer activity solely
688 depends on p53 binding and that p53 motifs are the strongest predictor of high enhancer activity (Verfaillie
689 et al., 2016; Younger and Rinn, 2017). While global MPRA analyses of ATF4-dependent regulatory
690 elements have not been reported, our results suggest that like p53, ATF4 may not require other transcription
691 factors to induce stress-dependent enhancer activity. This model is attractive as the regulatory activity of
692 stress-dependent transcription factors would remain robust across contexts. Although they appear
693 unnecessary for stress-mediated induction, transcription factor motifs (ETV6, AP1:BACH1,
694 GLIS3/POU6F) identified via saturating mutagenesis modulate *GADD45A* enhancer activity in unstressed
695 conditions. These results also provide a context where additional transcription factors regulate p53- or
696 ATF4-bound enhancers and suggest that differential enhancer "grammar" may be needed for basal versus
697 stress-dependent transcriptional regulation.

p53-dependent enhancers may rely on other transcription factors in certain contexts, like with varied cell lineage-dependent chromatin structure (Karsli Uzunbas et al., 2019). One caveat to MPRA studies is they can lack chromatin context that might mask the requirement for other transcription factors that alter chromatin accessibility. Additionally, enhancers display cell lineage-dependent activity due to differential expression of these transcription factors and cofactors. These caveats for MPRA studies are also relevant for our identification of shared gene targets between the p53 and ISR gene networks. Our global analyses was limited to one colon carcinoma cell line, but recent studies have identified previously underappreciated cell lineage-dependent p53 transcriptional networks (Andrysik et al., 2017; Nguyen et al., 2018; Fischer, 2019; Karsli Uzunbas et al., 2019). A full analysis of cell lineage-specificity has not been directly explored in the ATF4-dependent ISR. Thus, the shared gene network between the p53 and ISR gene networks is likely more expansive than is reported here. Our results identify autonomous activity of p53 and ATF4 during stress-dependent enhancer activation and gene regulation, and certainly additional exploration of context-dependent enhancer activity and shared gene targets is required,

Data Availability

The data that support the findings of this study are openly available in Gene Expression Omnibus (GEO) at https://www.ncbi.nlm.nih.gov/geo/, reference numbers GSE211244 (RNAseq), GSE211264 (CUT&RUN), GSE226617 (STARRSeq mutagenesis screen).

Acknowledgments

The authors would like to thank the University at Albany Center for Functional Genomics for sequencing and analytical support. SAD was supported by a University at Albany RNA Institute Fellowship. This work was supported by NIH NIGMS R35 GM138120.

724 **Figure Legends**

725

726 **Figure 1. ATF3 is a p53 target gene that is activated via the ISR in a p53-independent manner.**

727 Western Blot analysis of A) ATF3 and B) p53 with GAPDH as a loading control in HCT116 p53 WT (left)
728 and p53 null cells (right) following a 6h treatment with DMSO, 5 μM Nutlin-3A (NUT), 100 μM etoposide
729 (ETOP), 2 μM tunicamycin (TM) or 2mM histidinol (HisOH). Gene expression analysis of the C) *ATF3*
730 gene D) *CDKN1A* gene and E) *ASNS* gene in HCT116 p53 WT (black) and HCT116 p53 null (pink) cells
731 in response to 6h treatment with stimuli. All statistical comparisons were computed using a one-way
732 ANOVA test. *p<0.05, **p<0.01, ***p<0.001, ****p<0.0001.

733

734 **Figure 2. ATF4 and p53 independently regulate expression of *ATF3*.**

735 ATF4 protein (A-C) and mRNA (D-F) expression analysis by western blot and qRT-PCR, respectively, in
736 HCT116 WT or p53 null cells (A, D), with shRNA constructs targeting control region (control shRNA) or
737 *ATF4* (ATF4 shRNA) (B, E), or HAP1 WT or HAP1 ATF4KO cells (C, F). Gene expression analysis of
738 *ATF3* (G, H) or *ASNS* (I, J) in HCT116 ATF4 shRNA cells (G, I) or HAP1 ATF4KO cells (H, J). Cells
739 were harvested 6h post-treatment with DMSO, 10 μM nutlin-3A (NUT), 100 μM etoposide (ETOP), 2 μM
740 tunicamycin (TM) or 2 mM histidinol (HisOH). All statistical comparisons were computed using a one-
741 way ANOVA test. *p<0.05, **p<0.01, ***p<0.001, ****p<0.0001.

742

743 **Figure 3. ATF4 and p53 occupy distinct regulatory regions in the *ATF3* gene locus.**

744 A) Known motif enrichment analysis of the high-confidence peak set reveals the predicted ATF4 motif as
745 the most highly enriched motif within this dataset. B) *de novo* motif analysis of high-confidence peak set
746 shows enrichment of ATF4 motif. C) Enrichment of CUT&RUN sequencing tags for the 7,723 high-
747 confidence ATF4 peaks after 6h drug treatments as indicated from -1 kb and +1 kb from peak center. D)
748 Genome browser view of the *ATF3* gene locus displaying ATF4 CUT&RUN data (black) and p53 ChIP-
749 Seq data (green) (scaled to 1 as the maximum value for ATF4 or p53) following 6 h treatment with various

750 stress stimuli: DMSO (vehicle control), 5 μM nutlin-3A (NUTLIN), 100 μM etoposide (ETOP), 2 μM
751 tunicamycin (TM), or 2mM histidinol (HisOH). E-G) The top 5 most enriched results from *chiprenrich* for
752 ATF4 CUT&RUN high-confidence peaks (from this manuscript) or nutlin-induced p53 ChIP-seq peaks
753 (from (Andrysik et al., 2017)) for E) the mSigDB v6.0 Hallmark (Liberzon et al., 2015), F) KEGG v3.2.3
754 (Kanehisa et al., 2023), or G) REACTOME v61 (Gillespie et al., 2022) gene sets. *P*-values are $\log_{10}$ (1/
755 Bonferroni-corrected P-value). Full data tables for enrichment results can be found in Table S5.
756
757 **Figure 4. *ATF3* induction by the ISR does not require the upstream enhancer element bound by p53.**
758 A) Normalized luciferase values driven by the upstream *ATF3* DNase Hypersensitivity sites (DHS): ATF4-
759 bound DHS, p53-bound DHS, p53RE Mutant, and the minimal promoter (negative control), in response to
760 16h treatment with DMSO, 5 μM nutlin-3A (NUT) or 2 μM tunicamycin (Tm) in HCT116 p53 WT and
761 p53 null cells. B) Normalized luciferase values driven by the (-104/+36) *ATF3* promoter sequence (WT
762 *ATF3* promoter) and constructs containing mutations in specific ATF4 response elements: CARE, CRE,
763 CARE/CRE, in response to 16 h treatment with DMSO, 2 μM tunicamycin (Tm), or 2mM histidinol
764 (HisOH) in HAP1 parental and ATF4KO cells. Luciferase reporters with relevant motif positions and
765 sequences are illustrated above the corresponding bar chart (A-B), genomic locations of the *ATF3* promoter
766 and DHS are reported in Table S1. C) Genome browser view of the *ATF3* gene locus displaying the location
767 of dCas9-KRAB gRNA targets and the genomic coordinates spanning these targets relevant to panel D. D)
768 RT-qPCR analysis of the *ATF3* gene in response to 6 h treatment with DMSO, 100 μM etoposide (ETOP)
769 or 2 μM tunicamycin (TM) in HCT116 p53 WT cells where dCas9-KRAB is targeting regions at off-target
770 sites at a control FGF2 enhancer (blue) or intergenic region (orange and green), the p53-bound *ATF3*
771 enhancer element (purple) or *ATF3* promoter (red) for transcriptional repression. RT-qPCR analysis of the
772 E) *ASNS* gene, and F) *CDKN1A*/*p21* gene, following a 6h treatment with various stress stimuli. Statistical
773 comparisons for nascent expression levels were computed using a one-way ANOVA test. *$p<0.05$,
774 **$p<0.01$, ***$p<0.001$, ****$p<0.0001$.
775

776 **Figure 5. Global transcriptome analysis identifies common gene regulatory targets of the p53 GRN**
777 **and the ISR.**
778 A) Intersection of genes upregulated (any fold-change relative to DMSO, Bonferroni-adjusted P-value
779 <0.05) in HCT116 p53 WT cells treated with 5 μM nutlin-3A, 100 μM etoposide, 2 μM tunicamycin, and
780 2 μM histidinol, when compared to vehicle control (DMSO) for 6h. B) Bar plots representing a fraction of
781 genes identified from the RNA-seq experiment as upregulated (yellow), downregulated (blue), or not
782 regulated (white) in response to various stimuli that have a CUT&RUN-defined ATF4 binding event within
783 a binned distance indicated on the *x*-axis. C) Causal Inference Engine predictions of the top 5 putative
784 upstream regulators of genes from the TRRUST database induced by tunicamycin, histidinol, or etoposide
785 treatment (as determined using the Fisher's exact test for significance) (Han et al., 2018; Farahmand et al.,
786 2019). Complete Causal Inference Engine results for the STRING database for both WT and HCT116 p53
787 null cells can be found in Fig. S3 and Table S4 (Szklarczyk et al., 2022). D) Gene ontology analysis of the
788 genes commonly upregulated and downregulated (any fold-change relative to DMSO, Bonferroni-adjusted
789 P-value <0.05), in response to various stress stimuli. E) Heatmap and hierarchical clustering results (one
790 minus Pearson, average linkage) displaying fold change values for the 26 common targets identified in
791 panel A. F) Table displaying the gene symbols for the 26 common target Ensembl gene IDs identified in
792 panel A and matching row names in panel E. Genes validated in Fig. 6 by RT-qPCR are depicted in bold
793 font.
794
795 **Figure 6. Parallel stress-dependent networks converge at activation of a common set of target genes.**
796 RT-qPCR analysis of the *ATF3, GADD45A*, *SESN2,* and *GDF15* gene in A-D) HCT116 p53 WT and p53
797 null cells, E-H) MCF10A p53 WT and p53 null cells, and I-L) HAP1 parental and ATF4KO cells, following
798 a 6h treatment with DMSO, 100 μM etoposide (ETOP), or 2 μM Tunicamycin (Tm). All statistical
799 comparisons were computed using a one-way ANOVA test. *p<0.05, **p<0.01, ***p<0.001,
800 ****p<0.0001.
801

802 **Figure 7. *GADD45A* as a reporter system to study DDR- and ISR-dependent enhancers.**
803 A) Genome browser view with *GADD45A* locus displaying ATF4 CUT&RUN and p53 ChIP-Seq data
804 (Andrysik et al., 2017) in HCT116 WT cell line following 6h treatment with DMSO, 2 mM histidinol
805 (HisOH), 2 μM Tunicamycin (TM), and 5 μM nutlin-3A (NUT). Putative p53RE, ATF4 motif and
806 GADD45A intron 3 enhancer locations are indicated on the bottom, DNaseI hypersensitive sites (DHS) are
807 marked in grey/black. B) Schematic representation of the *GADD45A-nLuc* reporter construct with relevant
808 enhancer sequence motifs highlighted in panel C. D) Normalized luciferase expression values using
809 *GADD45A-nLuc* reporter transfected into HCT116 wt cell line and 16h treatment with DMSO, nutlin-3A
810 and tunicamycin as indicated in the legend. Reporter constructs included wild type, a negative control with
811 250 bp enhancer deletion ('No Enhancer') and various ATF4, AP1 and p53RE motif mutations alone or in
812 combination as indicated in the table below ('wt' or 'mutant' in grey). Specific mutations in motifs are
813 indicated in panel C. Statistical comparisons were generated using one-way ANOVA: * $p<0.05$, ** $p<0.01$,
814 *** $p< 0.001$, **** $p<0.0001$.
815
816 **Figure 8. Nucleotide resolution of *GADD45A* enhancer sequence critical for promoter activation**
817 **function.** A) Schematic illustrating *GADD45A* 250 nt enhancer mutagenesis screen using the STARRSeq
818 system (hSTARRSeq_ORI). Substitutions and deletions of every nucleotide position are depicted as 'X';
819 p53RE in blue; open reading frame as 'ORF'; polyadenylation site as 'polyA'. B) Heatmap representing
820 expression mediated by each enhancer variant relative to the wild-type enhancer from the same cell line
821 and treatment condition. Relative position in the enhancer (1-250 nt) is indicated on the *x*-axis. Each
822 deletion ('Del') or base substitution ('A', 'C', 'G', 'T') is indicated as a row label. 'Grey' color in row 'Del'
823 indicates a redundant position when >1 consecutive base is identical. Relevant motifs discussed in the text
824 are highlighted (red dashed line) including: *GADD45A* native motif sequence, relative position, name
825 ('p53RE', 'AP1') and PWM logos (JASPAR 2022 (Castro-Mondragon et al., 2022)) are in panel C. Cell
826 lines and treatment conditions are indicated above each heatmap.
827

828 **Figure 9. Other STARRSeq-identified motifs contribute only to basal *GADD45A* enhancer activity.**
829 A) Schematic representation of the *GADD45A-nLuc* reporter construct with relevant enhancer sequence
830 motifs highlighted in panel B. C) Normalized luciferase expression values using *GADD45A-nLuc* reporter
831 transfected into HCT116 WT cell line and 16h treatment with DMSO, nutlin-3A and tunicamycin as
832 indicated in the legend. Reporter constructs included wild-type (wt) construct, 250 bp enhancer deletion
833 ('No Enhancer') as a negative control and various predicted transcription factor motif mutations as
834 indicated on the *x*-axis. Specific mutations in transcription factor motifs based on the STARRSeq screen
835 are indicated in panel B. Statistical comparisons were generated using one-way ANOVA: * $p<0.05$, **
836 $p<0.01$, *** $p< 0.001$, **** $p<0.0001$.
837
838 **Figure S1.**
839 A) Intersection of ATF4 CUT&RUN peaks for the three biological replicates of HCT116 p53 WT cells
840 treated with 2 μM tunicamycin for 6h. B) Intersection of ATF4 CUT&RUN peaks for the three biological
841 replicates of HCT116 p53 WT cells treated with 2 mM histidinol for 6 hrs. C) A set of high-confidence
842 ISR-activated ATF4 binding events created by considering only peaks called out from 5 out of the 6
843 experiments with ISR-activating treatments: 2 μM tuncamycin and 2 mM histidinol. D) Genome browser
844 view of the *ASNS* gene locus displaying ATF4 CUT&RUN data (black) and p53 ChIP-Seq data (green) in
845 HCT116 p53 WT cells following 6 h treatment with various stress stimuli, including: DMSO (vehicle
846 control), 5 μM nutlin-3A (NUTLIN), 100 μM etoposide (ETOP), 2 μM tunicamycin (TM), and 2mM
847 histidinol (HisOH).
848
849 **Figure S2.**
850 RNASeq analysis of differential gene expression in HCT116 WT and p53 null cell lines in response 5 μM
851 nutlin-3A (A, E), 100 μM etoposide (B, F), 2 μM tunicamycin (C, G), or 2mM histidinol (D, H), compared
852 to vehicle control (DMSO). Gene ontology analysis of the genes upregulated (A-D) and downregulated (E-
853 H) in response to treatments. (I-L) Enhanced volcano plots displaying differential gene expression in

854 HCT116 WT cells treated stimuli as described above. Number of genes (n) upregulated or downregulated
855 in each condition is indicated on the left side or the right side of each volcano plot, respectively.
856
857 **Figure S3. Causal Inference Engine enrichment of putative upstream regulators of stress-induced**
858 **gene expression in WT and p53 null HCT116 cells.** A) Results of the top 5 most enriched upstream
859 regulators from the TRRUST database of tunicamycin, histidinol, or etoposide-induced genes in HCT116
860 p53 null cells (p-value derived from the Fisher's Exact test for enrichment). Results of the top 5 most
861 enriched upstream regulators from the STRING database for genes induced in (B) HCT116 WT or (C)
862 HCT116 p53 null cells from Causal Inference Engine (p-value derived from the Quaternary Scoring statistic
863 (QS) from (Fakhry et al., 2016)). Plots were generated with GSEApy (Fang et al., 2023).
864
865 **Figure S4. Comparison of *GADD45A-nLuc* reporter expression in the presence or absence of T2A**
866 **skipping peptide and/or hPEST degradation tag.** A) Schematic representation of various *GADD45A-*
867 *nLuc* reporter constructs with T2A or hPEST included in the 3' end. B) Normalized luciferase expression
868 values from *GADD45A-nLuc* reporters transfected into HCT116 WT cell line and 16h treatment with
869 DMSO, nutlin-3A and tunicamycin as indicated in the legend. Presence ('+') or absence (grey) of T2A or
870 hPEST tags are indicated in the table below.
871
872 **Figure S5. Nucleotide resolution of *GADD45A* enhancer sequence critical for promoter activation**
873 **function (extended Fig. 8B).** Heatmap representing expression mediated by each enhancer variant relative
874 to the wild-type enhancer from the same cell line and treatment condition. Relative position in the enhancer
875 (1-250 nt) is indicated on the *x*-axis. Each deletion ('Del') or base substitution ('A', 'C', 'G', 'T') is
876 indicated as a row label. 'Grey' color in row 'Del' indicates a redundant position when >1 consecutive base
877 is identical. Relevant motifs discussed in the text are highlighted (red dashed line) including: *GADD45A*
878 native motif sequence, relative position, name ('HNF4G', 'ATF4', 'ZNF93', 'ETV6', 'TWIST1',
879 'GATA1', 'ZNF136', 'GLIS3/POU6F2') and PWM logos (JASPAR 2022 (Castro-Mondragon et al.,

880 2022)). Cell lines and treatment conditions are indicated above each heatmap. (Top Row) Barplot
881 highlighting SNPs found in *GADD45A* enhancer region from db155SNP database with expression values
882 from HCT116 WT, DMSO experiment.
883
884 **Table S1. List of plasmids and oligonucleotides used in this study.**

885 **Table S2. Full list of DEseq2-derived differential gene expression values for HCT116 WT and p53**
886 **null cells treated with vehicle control (DMSO) relative to nutlin-3A, etoposide, tunicamycin, or**
887 **histidinol treatments.**
888
889 **Table S3. Full Gene Ontology Enrichment results from Figure 5 and Figure S2.**
890
891 **Table S4. Complete Causal Inference Engine analysis of putative upstream regulators of genes**
892 **induced by etoposide, tunicamycin, or histidinol in WT or p53 null HCT116 cells.**
893
894 **Table S5. Full *chipenrich* results using KEGG, HALLMARK and REACTOME databases.**

895 **References**

896

897 Advani, V. M., and Ivanov, P. (2019). Translational Control under Stress: Reshaping the Translatome.
898 *BioEssays* 41, 1900009. doi: 10.1002/bies.201900009.

899 Aguilar-Recarte, D., Barroso, E., Gumà, A., Pizarro-Delgado, J., Peña, L., Ruart, M., et al. (2021).
900 GDF15 mediates the metabolic effects of PPARβ/δ by activating AMPK. *Cell Rep.* 36, 109501.
901 doi: 10.1016/j.celrep.2021.109501.

902 Andreeff, M., Kelly, K. R., Yee, K., Assouline, S., Strair, R., Popplewell, L., et al. (2016). Results of the
903 Phase I Trial of RG7112, a Small-Molecule MDM2 Antagonist in Leukemia. *Clin. Cancer Res.*
904 22, 868–876. doi: 10.1158/1078-0432.CCR-15-0481.

905 Andrysik, Z., Galbraith, M. D., Guarnieri, A. L., Zaccara, S., Sullivan, K. D., Pandey, A., et al. (2017).
906 Identification of a core TP53 transcriptional program with highly distributed tumor suppressive
907 activity. *Genome Res.* 27, 1645–1657. doi: 10.1101/gr.220533.117.

908 Andrysik, Z., Sullivan, K. D., Kieft, J. S., and Espinosa, J. M. (2022). PPM1D suppresses p53-dependent
909 transactivation and cell death by inhibiting the Integrated Stress Response. *Nat. Commun.* 13,
910 7400. doi: 10.1038/s41467-022-35089-5.

911 Aziz, M. H., Shen, H., and Maki, C. G. (2011). Acquisition of p53 mutations in response to the non-
912 genotoxic p53 activator Nutlin-3. *Oncogene* 30, 4678–4686. doi: 10.1038/onc.2011.185.

913 Bejjani, F., Evanno, E., Zibara, K., Piechaczyk, M., and Jariel-Encontre, I. (2019). The AP-1
914 transcriptional complex: Local switch or remote command? *Biochim. Biophys. Acta BBA - Rev.*
915 *Cancer* 1872, 11–23. doi: 10.1016/j.bbcan.2019.04.003.

916 Bray, N. L., Pimentel, H., Melsted, P., and Pachter, L. (2016). Near-optimal probabilistic RNA-seq
917 quantification. *Nat. Biotechnol.* 34, 525–527. doi: 10.1038/nbt.3519.

918 Budanov, A. V., and Karin, M. (2008). p53 Target Genes Sestrin1 and Sestrin2 Connect Genotoxic Stress
919 and mTOR Signaling. *Cell* 134, 451–460. doi: 10.1016/j.cell.2008.06.028.

920 Bushnell, B., Rood, J., and Singer, E. (2017). BBMerge – Accurate paired shotgun read merging via
921 overlap. *PLOS ONE* 12, e0185056. doi: 10.1371/journal.pone.0185056.

922 Bykov, V. J. N., Eriksson, S. E., Bianchi, J., and Wiman, K. G. (2018). Targeting mutant p53 for efficient
923 cancer therapy. *Nat. Rev. Cancer* 18, 89–102. doi: 10.1038/nrc.2017.109.

924 Castro-Mondragon, J. A., Riudavets-Puig, R., Rauluseviciute, I., Berhanu Lemma, R., Turchi, L., Blanc-
925 Mathieu, R., et al. (2022). JASPAR 2022: the 9th release of the open-access database of
926 transcription factor binding profiles. *Nucleic Acids Res.* 50, D165–D173. doi:
927 10.1093/nar/gkab1113.

928 Catizone, A. N., Uzunbas, G. K., Celadova, P., Kuang, S., Bose, D., and Sammons, M. A. (2020). Locally
929 acting transcription factors regulate p53-dependent cis-regulatory element activity. *Nucleic Acids*
930 *Res.* 48, 4195–4213. doi: 10.1093/nar/gkaa147.

931 Chaudhari, H. G., and Cohen, B. A. (2018). Local sequence features that influence AP-1 cis-regulatory
932 activity. *Genome Res.* 28, 171–181. doi: 10.1101/gr.226530.117.

933 Chavel, C. A., Dionne, H. M., Birkaya, B., Joshi, J., and Cullen, P. J. (2010). Multiple Signals Converge
934 on a Differentiation MAPK Pathway. *PLoS Genet.* 6, e1000883. doi:
935 10.1371/journal.pgen.1000883.

936 Chen, B. P., Wolfgang, C. D., and Hai, T. (1996). Analysis of ATF3, a transcription factor induced by
937 physiological stresses and modulated by gadd153/Chop10. *Mol. Cell. Biol.* 16, 1157–1168. doi:
938 10.1128/MCB.16.3.1157.

939 Chen, E. Y., Tan, C. M., Kou, Y., Duan, Q., Wang, Z., Meirelles, G. V., et al. (2013). Enrichr: interactive
940 and collaborative HTML5 gene list enrichment analysis tool. *BMC Bioinformatics* 14, 128. doi:
941 10.1186/1471-2105-14-128.

942 Chen, H., Pan, Y.-X., Dudenhausen, E. E., and Kilberg, M. S. (2004). Amino Acid Deprivation Induces
943 the Transcription Rate of the Human Asparagine Synthetase Gene through a Timed Program of
944 Expression and Promoter Binding of Nutrient-responsive Basic Region/Leucine Zipper
945 Transcription Factors as Well as Localized Histone Acetylation. *J. Biol. Chem.* 279, 50829–
946 50839. doi: 10.1074/jbc.M409173200.

947 Chin, P. L., Momand, J., and Pfeifer, G. P. (1997). In vivo evidence for binding of p53 to consensus
948 binding sites in the p21 and GADD45 genes in response to ionizing radiation. *Oncogene* 15, 87–
949 99. doi: 10.1038/sj.onc.1201161.

950 Choi, J., Lysakovskaia, K., Stik, G., Demel, C., Söding, J., Tian, T. V., et al. (2021). Evidence for
951 additive and synergistic action of mammalian enhancers during cell fate determination. *eLife* 10,
952 e65381. doi: 10.7554/eLife.65381.

953 Chowdhury, P., Lin, G. E., Liu, K., Song, Y., Lin, F.-T., and Lin, W.-C. (2014). Targeting TopBP1 at a
954 convergent point of multiple oncogenic pathways for cancer therapy. *Nat. Commun.* 5, 5476. doi:
955 10.1038/ncomms6476.

956 Coronel, L., Häckes, D., Schwab, K., Riege, K., Hoffmann, S., and Fischer, M. (2022). p53-mediated
957 AKT and mTOR inhibition requires RFX7 and DDIT4 and depends on nutrient abundance.
958 *Oncogene* 41, 1063–1069. doi: 10.1038/s41388-021-02147-z.

959 Daino, K., Ichimura, S., and Nenoi, M. (2006). Both the basal transcriptional activity of the GADD45A
960 gene and its enhancement after ionizing irradiation are mediated by AP-1 element. *Biochim.*
961 *Biophys. Acta BBA - Gene Struct. Expr.* 1759, 458–469. doi: 10.1016/j.bbaexp.2006.09.005.

962 Dey, S., Baird, T. D., Zhou, D., Palam, L. R., Spandau, D. F., and Wek, R. C. (2010). Both
963 Transcriptional Regulation and Translational Control of ATF4 Are Central to the Integrated
964 Stress Response *. *J. Biol. Chem.* 285, 33165–33174. doi: 10.1074/jbc.M110.167213.

965 Di Marcantonio, D., Martinez, E., Kanefsky, J. S., Huhn, J. M., Gabbasov, R., Gupta, A., et al. (2021).
966 ATF3 coordinates serine and nucleotide metabolism to drive cell cycle progression in acute
967 myeloid leukemia. *Mol. Cell* 81, 2752-2764.e6. doi: 10.1016/j.molcel.2021.05.008.

968 Ding, W.-X., Ni, H.-M., Gao, W., Hou, Y.-F., Melan, M. A., Chen, X., et al. (2007). Differential Effects
969 of Endoplasmic Reticulum Stress-induced Autophagy on Cell Survival*. *J. Biol. Chem.* 282,
970 4702–4710. doi: 10.1074/jbc.M609267200.

971 Ebert, S. M., Al-Zougbi, A., Bodine, S. C., and Adams, C. M. (2019). Skeletal Muscle Atrophy:
972 Discovery of Mechanisms and Potential Therapies. *Physiology* 34, 232–239. doi:
973 10.1152/physiol.00003.2019.

974 el-Deiry, W. S., Kern, S. E., Pietenpol, J. A., Kinzler, K. W., and Vogelstein, B. (1992). Definition of a
975 consensus binding site for p53. *Nat. Genet.* 1, 45–49. doi: 10.1038/ng0492-45.

976 el-Deiry, W. S., Tokino, T., Velculescu, V. E., Levy, D. B., Parsons, R., Trent, J. M., et al. (1993).
977 WAF1, a potential mediator of p53 tumor suppression. *Cell* 75, 817–825. doi: 10.1016/0092-
978 8674(93)90500-p.

979 Fakhry, C. T., Choudhary, P., Gutteridge, A., Sidders, B., Chen, P., Ziemek, D., et al. (2016). Interpreting
980 transcriptional changes using causal graphs: new methods and their practical utility on public
981 networks. *BMC Bioinformatics* 17, 318. doi: 10.1186/s12859-016-1181-8.

982 Fang, Z., Liu, X., and Peltz, G. (2023). GSEApy: a comprehensive package for performing gene set
983 enrichment analysis in Python. *Bioinforma. Oxf. Engl.* 39, btac757. doi:
984 10.1093/bioinformatics/btac757.

985 Farahmand, S., O'Connor, C., Macoska, J. A., and Zarringhalam, K. (2019). Causal Inference Engine: a
986 platform for directional gene set enrichment analysis and inference of active transcriptional
987 regulators. *Nucleic Acids Res.* 47, 11563–11573. doi: 10.1093/nar/gkz1046.

988 Fischer, M. (2019). Conservation and divergence of the p53 gene regulatory network between mice and
989 humans. *Oncogene*. doi: 10.1038/s41388-019-0706-9.

990 Fu, L., and Kilberg, M. S. (2013). Elevated cJUN expression and an ATF/CRE site within the ATF3
991 promoter contribute to activation of ATF3 transcription by the amino acid response. *Physiol.*
992 *Genomics* 45, 127–137. doi: 10.1152/physiolgenomics.00160.2012.

993 Gambardella, G., Staiano, L., Moretti, M. N., De Cegli, R., Fagnocchi, L., Di Tullio, G., et al. (2020).
994 GADD34 is a modulator of autophagy during starvation. *Sci. Adv.* 6, eabb0205. doi:
995 10.1126/sciadv.abb0205.

996 Garaeva, A. A., Kovaleva, I. E., Chumakov, P. M., and Evstafieva, A. G. (2016). Mitochondrial
997 dysfunction induces *SESN* 2 gene expression through Activating Transcription Factor 4. *Cell*
998 *Cycle* 15, 64–71. doi: 10.1080/15384101.2015.1120929.

999 Gilbert, L. A., Larson, M. H., Morsut, L., Liu, Z., Brar, G. A., Torres, S. E., et al. (2013). CRISPR-
1000 Mediated Modular RNA-Guided Regulation of Transcription in Eukaryotes. *Cell* 154, 442–451.
1001 doi: 10.1016/j.cell.2013.06.044.

1002 Gillespie, M., Jassal, B., Stephan, R., Milacic, M., Rothfels, K., Senff-Ribeiro, A., et al. (2022). The
1003 reactome pathway knowledgebase 2022. *Nucleic Acids Res.* 50, D687–D692. doi:
1004 10.1093/nar/gkab1028.

1005 Hai, T. (2006). "The ATF Transcription Factors in Cellular Adaptive Responses," in *Gene Expression*
1006 *and Regulation*, ed. J. Ma (New York, NY: Springer New York), 329–340. doi: 10.1007/978-0-
1007 387-40049-5_20.

1008 Hai, T., and Curran, T. (1991). Cross-family dimerization of transcription factors Fos/Jun and ATF/CREB
1009 alters DNA binding specificity. *Proc. Natl. Acad. Sci.* 88, 3720–3724. doi:
1010 10.1073/pnas.88.9.3720.

1011 Hai, T., Wolfgang, C. D., Marsee, D. K., Allen, A. E., and Sivaprasad, U. (1999). ATF3 and stress
1012 responses. *Gene Expr.* 7, 321–335.

1013 Hai, T., Wolford, C. C., and Chang, Y.-S. (2010). ATF3, a hub of the cellular adaptive-response network,
1014 in the pathogenesis of diseases: is modulation of inflammation a unifying component? *Gene Expr.*
1015 15, 1–11. doi: 10.3727/105221610x12819686555015.

1016 Han, H., Cho, J.-W., Lee, S., Yun, A., Kim, H., Bae, D., et al. (2018). TRRUST v2: an expanded
1017 reference database of human and mouse transcriptional regulatory interactions. *Nucleic Acids*
1018 *Res.* 46, D380–D386. doi: 10.1093/nar/gkx1013.

1019 Han, J., Back, S. H., Hur, J., Lin, Y.-H., Gildersleeve, R., Shan, J., et al. (2013). ER-stress-induced
1020 transcriptional regulation increases protein synthesis leading to cell death. *Nat. Cell Biol.* 15,
1021 481–490. doi: 10.1038/ncb2738.

1022 Hashimoto, Y., Zhang, C., Kawauchi, J., Imoto, I., Adachi, M. T., Inazawa, J., et al. (2002). An
1023 alternatively spliced isoform of transcriptional repressor ATF3 and its induction by stress stimuli.
1024 *Nucleic Acids Res.* 30, 2398–2406. doi: 10.1093/nar/30.11.2398.

1025 Hernandez Borrero, L., Dicker, D. T., Santiago, J., Sanders, J., Tian, X., Ahsan, N., et al. (2021). A subset
1026 of CB002 xanthine analogs bypass p53-signaling to restore a p53 transcriptome and target an S-
1027 phase cell cycle checkpoint in tumors with mutated-p53. *eLife* 10, e70429. doi:
1028 10.7554/eLife.70429.

1029 Jensen, M. (2003). Reduced hepatic tumor incidence in cyclin G1-deficient mice. *Hepatology* 37, 862–
1030 870. doi: 10.1053/jhep.2003.50137.

1031 Jiang, H.-Y., Wek, S. A., McGrath, B. C., Lu, D., Hai, T., Harding, H. P., et al. (2004). Activating
1032 transcription factor 3 is integral to the eukaryotic initiation factor 2 kinase stress response. *Mol.*
1033 *Cell. Biol.* 24, 1365–1377. doi: 10.1128/MCB.24.3.1365-1377.2004.

1034 Kanehisa, M., Furumichi, M., Sato, Y., Kawashima, M., and Ishiguro-Watanabe, M. (2023). KEGG for
1035 taxonomy-based analysis of pathways and genomes. *Nucleic Acids Res.* 51, D587–D592. doi:
1036 10.1093/nar/gkac963.

1037 Karsli Uzunbas, G., Ahmed, F., and Sammons, M. A. (2019). Control of p53-dependent transcription and
1038 enhancer activity by the p53 family member p63. *J. Biol. Chem.* doi: 10.1074/jbc.RA119.007965.

1039 Kastan, M. B., Onyekwere, O., Sidransky, D., Vogelstein, B., and Craig, R. W. (1991). Participation of
1040 p53 protein in the cellular response to DNA damage. *Cancer Res.* 51, 6304–6311.

1041 Kilberg, M. S., Shan, J., and Su, N. (2009). ATF4-dependent transcription mediates signaling of amino
1042 acid limitation. *Trends Endocrinol. Metab.* 20, 436–443. doi: 10.1016/j.tem.2009.05.008.

1043 Kim, D., Paggi, J. M., Park, C., Bennett, C., and Salzberg, S. L. (2019). Graph-based genome alignment
1044 and genotyping with HISAT2 and HISAT-genotype. *Nat. Biotechnol.* 37, 907–915. doi:
1045 10.1038/s41587-019-0201-4.

1046 Kim, D. S., Risca, V. I., Reynolds, D. L., Chappell, J., Rubin, A. J., Jung, N., et al. (2021). The dynamic,
1047 combinatorial cis-regulatory lexicon of epidermal differentiation. *Nat. Genet.* 53, 1564–1576. doi:
1048 10.1038/s41588-021-00947-3.

1049 Kim, S., and Wysocka, J. (2023). Deciphering the multi-scale, quantitative cis-regulatory code. *Mol. Cell*
1050 83, 373–392. doi: 10.1016/j.molcel.2022.12.032.

1051 Kocik, J., Machula, M., Wisniewska, A., Surmiak, E., Holak, T. A., and Skalniak, L. (2019). Helping the
1052 Released Guardian: Drug Combinations for Supporting the Anticancer Activity of HDM2
1053 (MDM2) Antagonists. *Cancers* 11, 1014. doi: 10.3390/cancers11071014.

1054 Ku, H.-C., and Cheng, C.-F. (2020). Master Regulator Activating Transcription Factor 3 (ATF3) in
1055 Metabolic Homeostasis and Cancer. *Front. Endocrinol.* 11, 556. doi: 10.3389/fendo.2020.00556.

1056 Kuleshov, M. V., Jones, M. R., Rouillard, A. D., Fernandez, N. F., Duan, Q., Wang, Z., et al. (2016).
1057 Enrichr: a comprehensive gene set enrichment analysis web server 2016 update. *Nucleic Acids*
1058 *Res.* 44, W90–W97. doi: 10.1093/nar/gkw377.

1059 Li, A., Zhao, F., Zhao, Y., Liu, H., and Wang, Z. (2021). ATF4-mediated GDF15 suppresses LPS-
1060 induced inflammation and MUC5AC in human nasal epithelial cells through the PI3K/Akt
1061 pathway. *Life Sci.* 275, 119356. doi: 10.1016/j.lfs.2021.119356.

1062 Liberzon, A., Birger, C., Thorvaldsdóttir, H., Ghandi, M., Mesirov, J. P., and Tamayo, P. (2015). The
1063 Molecular Signatures Database (MSigDB) hallmark gene set collection. *Cell Syst.* 1, 417–425.
1064 doi: 10.1016/j.cels.2015.12.004.

1065 Loayza-Puch, F., Drost, J., Rooijers, K., Lopes, R., Elkon, R., and Agami, R. (2013). p53 induces
1066 transcriptional and translational programs to suppress cell proliferation and growth. *Genome Biol.*
1067 14, R32. doi: 10.1186/gb-2013-14-4-r32.

1068 Lockhart, S. M., Saudek, V., and O'Rahilly, S. (2020). GDF15: A Hormone Conveying Somatic Distress
1069 to the Brain. *Endocr. Rev.* 41, bnaa007. doi: 10.1210/endrev/bnaa007.

1070 Lopez, R. G., Carron, C., Oury, C., Gardellin, P., Bernard, O., and Ghysdael, J. (1999). TEL Is a
1071 Sequence-specific Transcriptional Repressor *. *J. Biol. Chem.* 274, 30132–30138. doi:
1072 10.1074/jbc.274.42.30132.

1073 Love, M. I., Huber, W., and Anders, S. (2014). Moderated estimation of fold change and dispersion for
1074 RNA-seq data with DESeq2. *Genome Biol.* 15, 550. doi: 10.1186/s13059-014-0550-8.

1075 Lu, D., Wolfgang, C. D., and Hai, T. (2006). Activating transcription factor 3, a stress-inducible gene,
1076 suppresses Ras-stimulated tumorigenesis. *J. Biol. Chem.* 281, 10473–10481. doi:
1077 10.1074/jbc.M509278200.

1078 Mann, I. K., Chatterjee, R., Zhao, J., He, X., Weirauch, M. T., Hughes, T. R., et al. (2013). CG
1079 methylated microarrays identify a novel methylated sequence bound by the CEBPB|ATF4
1080 heterodimer that is active in vivo. *Genome Res.* 23, 988–997. doi: 10.1101/gr.146654.112.

1081 Mantovani, F., Collavin, L., and Del Sal, G. (2019). Mutant p53 as a guardian of the cancer cell. *Cell*
1082 *Death Differ.* 26, 199–212. doi: 10.1038/s41418-018-0246-9.

1083 Margolin, J. F., Friedman, J. R., Meyer, W. K., Vissing, H., Thiesen, H. J., and Rauscher, F. J. (1994).
1084 Krüppel-associated boxes are potent transcriptional repression domains. *Proc. Natl. Acad. Sci. U.*
1085 *S. A.* 91, 4509–4513. doi: 10.1073/pnas.91.10.4509.

1086 Menendez, D., Inga, A., Snipe, J., Krysiak, O., Schönfelder, G., and Resnick, M. A. (2007). A single-
1087 nucleotide polymorphism in a half-binding site creates p53 and estrogen receptor control of
1088 vascular endothelial growth factor receptor 1. *Mol. Cell. Biol.* 27, 2590–2600. doi:
1089 10.1128/MCB.01742-06.

1090 Moder, M., Velimezi, G., Owusu, M., Mazouzi, A., Wiedner, M., Ferreira da Silva, J., et al. (2017).
1091 Parallel genome-wide screens identify synthetic viable interactions between the BLM helicase
1092 complex and Fanconi anemia. *Nat. Commun.* 8, 1238. doi: 10.1038/s41467-017-01439-x.

1093 Montesinos, P., Beckermann, B. M., Catalani, O., Esteve, J., Gamel, K., Konopleva, M. Y., et al. (2020).
1094 MIRROS: a randomized, placebo-controlled, Phase III trial of cytarabine ± idasanutlin in relapsed
1095 or refractory acute myeloid leukemia. *Future Oncol. Lond. Engl.* 16, 807–815. doi: 10.2217/fon-
1096 2020-0044.

1097 Muerdter, F., Boryń, Ł. M., Woodfin, A. R., Neumayr, C., Rath, M., Zabidi, M. A., et al. (2018).
1098 Resolving systematic errors in widely used enhancer activity assays in human cells. *Nat. Methods*
1099 15, 141–149. doi: 10.1038/nmeth.4534.

1100 Neumayr, C., Pagani, M., Stark, A., and Arnold, C. D. (2019). STARR-seq and UMI-STARR-seq:
1101 Assessing Enhancer Activities for Genome-Wide-, High-, and Low-Complexity Candidate
1102 Libraries. *Curr. Protoc. Mol. Biol.* 128, e105. doi: 10.1002/cpmb.105.

1103 Nguyen, T.-A. T., Grimm, S. A., Bushel, P. R., Li, J., Li, Y., Bennett, B. D., et al. (2018). Revealing a
1104 human p53 universe. *Nucleic Acids Res.* doi: 10.1093/nar/gky720.

1105 Osada, M., Park, H. L., Park, M. J., Liu, J.-W., Wu, G., Trink, B., et al. (2007). A p53-type response
1106 element in the GDF15 promoter confers high specificity for p53 activation. *Biochem. Biophys.*
1107 *Res. Commun.* 354, 913–918. doi: 10.1016/j.bbrc.2007.01.089.

1108 Pakos-Zebrucka, K., Koryga, I., Mnich, K., Ljujic, M., Samali, A., and Gorman, A. M. (2016). The
1109 integrated stress response. *EMBO Rep.* 17, 1374–1395. doi: 10.15252/embr.201642195.

1110 Pan, Y.-X., Chen, H., Thiaville, M. M., and Kilberg, M. S. (2007). Activation of the ATF3 gene through a
1111 co-ordinated amino acid-sensing response programme that controls transcriptional regulation of
1112 responsive genes following amino acid limitation. *Biochem. J.* 401, 299–307. doi:
1113 10.1042/BJ20061261.

1114 Podust, L. M., Krezel, A. M., and Kim, Y. (2001). Crystal Structure of the CCAAT Box/Enhancer-
1115 binding Protein β Activating Transcription Factor-4 Basic Leucine Zipper Heterodimer in the
1116 Absence of DNA *. *J. Biol. Chem.* 276, 505–513. doi: 10.1074/jbc.M005594200.

1117 Qi, L. S., Larson, M. H., Gilbert, L. A., Doudna, J. A., Weissman, J. S., Arkin, A. P., et al. (2013).
1118 Repurposing CRISPR as an RNA-guided platform for sequence-specific control of gene
1119 expression. *Cell* 152, 1173–1183. doi: 10.1016/j.cell.2013.02.022.

1120 Ramírez, F., Ryan, D. P., Grüning, B., Bhardwaj, V., Kilpert, F., Richter, A. S., et al. (2016). deepTools2:
1121 a next generation web server for deep-sequencing data analysis. *Nucleic Acids Res.* 44, W160–
1122 W165. doi: 10.1093/nar/gkw257.

1123 Shieh, S.-Y., Ikeda, M., Taya, Y., and Prives, C. (1997). DNA Damage-Induced Phosphorylation of p53
1124 Alleviates Inhibition by MDM2. *Cell* 91, 325–334. doi: 10.1016/S0092-8674(00)80416-X.

1125 Siu, F., Bain, P. J., LeBlanc-Chaffin, R., Chen, H., and Kilberg, M. S. (2002). ATF4 is a mediator of the
1126 nutrient-sensing response pathway that activates the human asparagine synthetase gene. *J. Biol.*
1127 *Chem.* 277, 24120–24127. doi: 10.1074/jbc.M201959200.

1128 Skene, P. J., and Henikoff, S. (2017). An efficient targeted nuclease strategy for high-resolution mapping
1129 of DNA binding sites. *eLife* 6, e21856. doi: 10.7554/eLife.21856.

1130 Smeenk, L., van Heeringen, S. J., Koeppel, M., van Driel, M. A., Bartels, S. J. J., Akkers, R. C., et al.
1131 (2008). Characterization of genome-wide p53-binding sites upon stress response. *Nucleic Acids*
1132 *Res.* 36, 3639–3654. doi: 10.1093/nar/gkn232.

1133 Smith, R. P., Taher, L., Patwardhan, R. P., Kim, M. J., Inoue, F., Shendure, J., et al. (2013). Massively
1134 parallel decoding of mammalian regulatory sequences supports a flexible organizational model.
1135 *Nat. Genet.* 45, 1021–1028. doi: 10.1038/ng.2713.

1136 Soneson, C., Love, M. I., and Robinson, M. D. (2015). Differential analyses for RNA-seq: transcript-level
1137 estimates improve gene-level inferences. *F1000Research* 4, 1521. doi:
1138 10.12688/f1000research.7563.1.

1139 Szak, S. T., Mays, D., and Pietenpol, J. A. (2001). Kinetics of p53 binding to promoter sites in vivo. *Mol.*
1140 *Cell. Biol.* 21, 3375–3386. doi: 10.1128/MCB.21.10.3375-3386.2001.

1141 Szklarczyk, D., Kirsch, R., Koutrouli, M., Nastou, K., Mehryary, F., Hachilif, R., et al. (2022). The
1142 STRING database in 2023: protein–protein association networks and functional enrichment
1143 analyses for any sequenced genome of interest. *Nucleic Acids Res.* 51, D638–D646. doi:
1144 10.1093/nar/gkac1000.

1145 Tameire, F., Verginadis, I. I., Leli, N. M., Polte, C., Conn, C. S., Ojha, R., et al. (2019). ATF4 couples
1146 MYC-dependent translational activity to bioenergetic demands during tumour progression. *Nat.*
1147 *Cell Biol.* 21, 889–899. doi: 10.1038/s41556-019-0347-9.

1148 Taniuchi, S., Miyake, M., Tsugawa, K., Oyadomari, M., and Oyadomari, S. (2016). Integrated stress
1149 response of vertebrates is regulated by four eIF2α kinases. *Sci. Rep.* 6, 32886. doi:
1150 10.1038/srep32886.

1151 Thakore, P. I., D'Ippolito, A. M., Song, L., Safi, A., Shivakumar, N. K., Kabadi, A. M., et al. (2015).
1152 Highly specific epigenome editing by CRISPR-Cas9 repressors for silencing of distal regulatory
1153 elements. *Nat. Methods* 12, 1143–1149. doi: 10.1038/nmeth.3630.

1154 Tian, X., Ahsan, N., Lulla, A., Lev, A., Abbosh, P., Dicker, D. T., et al. (2021). P53-independent partial
1155 restoration of the p53 pathway in tumors with mutated p53 through ATF4 transcriptional
1156 modulation by ERK1/2 and CDK9. *Neoplasia* 23, 304–325. doi: 10.1016/j.neo.2021.01.004.

1157 van Maanen, J. M. S., Retel, J., de Vries, J., and Pinedo, H. M. (1988). Mechanism of Action of
1158 Antitumor Drug Etoposide: A Review. *JNCI J. Natl. Cancer Inst.* 80, 1526–1533. doi:
1159 10.1093/jnci/80.19.1526.

1160 Vassilev, L. T., Vu, B. T., Graves, B., Carvajal, D., Podlaski, F., Filipovic, Z., et al. (2004). In Vivo
1161 Activation of the p53 Pathway by Small-Molecule Antagonists of MDM2. *Science* 303, 844–848.
1162 doi: 10.1126/science.1092472.

1163 Vattem, K. M., and Wek, R. C. (2004). Reinitiation involving upstream ORFs regulates ATF4 mRNA
1164 translation in mammalian cells. *Proc. Natl. Acad. Sci. U. S. A.* 101, 11269–11274. doi:
1165 10.1073/pnas.0400541101.

1166 Verfaillie, A., Svetlichnyy, D., Imrichova, H., Davie, K., Fiers, M., Atak, Z. K., et al. (2016). Multiplex
1167 enhancer-reporter assays uncover unsophisticated TP53 enhancer logic. *Genome Res.* 26, 882–
1168 895. doi: 10.1101/gr.204149.116.

1169 Vihervaara, A., Duarte, F. M., and Lis, J. T. (2018). Molecular mechanisms driving transcriptional stress
1170 responses. *Nat. Rev. Genet.* 19, 385–397. doi: 10.1038/s41576-018-0001-6.

1171 Weidenfeld-Baranboim, K., Hasin, T., Darlyuk, I., Heinrich, R., Elhanani, O., Pan, J., et al. (2009). The
1172 ubiquitously expressed bZIP inhibitor, JDP2, suppresses the transcription of its homologue
1173 immediate early gene counterpart, ATF3. *Nucleic Acids Res.* 37, 2194–2203. doi:
1174 10.1093/nar/gkp083.

1175 Welch, R. P., Lee, C., Imbriano, P. M., Patil, S., Weymouth, T. E., Smith, R. A., et al. (2014). ChIP-
1176 Enrich: gene set enrichment testing for ChIP-seq data. *Nucleic Acids Res.* 42, e105. doi:
1177 10.1093/nar/gku463.

1178 Xie, Z., Bailey, A., Kuleshov, M. V., Clarke, D. J. B., Evangelista, J. E., Jenkins, S. L., et al. (2021).
1179 Gene Set Knowledge Discovery with Enrichr. *Curr. Protoc.* 1. doi: 10.1002/cpz1.90.

1180 Yeo, N. C., Chavez, A., Lance-Byrne, A., Chan, Y., Menn, D., Milanova, D., et al. (2018). An enhanced
1181 CRISPR repressor for targeted mammalian gene regulation. *Nat. Methods* 15, 611–616. doi:
1182 10.1038/s41592-018-0048-5.

1183 Younger, S. T., and Rinn, J. L. (2017). p53 regulates enhancer accessibility and activity in response to
1184 DNA damage. *Nucleic Acids Res.* 45, 9889–9900. doi: 10.1093/nar/gkx577.

1185 Yu, X., Vazquez, A., Levine, A. J., and Carpizo, D. R. (2012). Allele-Specific p53 Mutant Reactivation.
1186 *Cancer Cell* 21, 614–625. doi: 10.1016/j.ccr.2012.03.042.

1187 Zaccara, S., Tebaldi, T., Pederiva, C., Ciribilli, Y., Bisio, A., and Inga, A. (2014). p53-directed
1188 translational control can shape and expand the universe of p53 target genes. *Cell Death Differ.* 21,
1189 1522–1534. doi: 10.1038/cdd.2014.79.

1190 Zeitlinger, J. (2020). Seven myths of how transcription factors read the cis-regulatory code. *Curr. Opin.*
1191 *Syst. Biol.* 23, 22–31. doi: 10.1016/j.coisb.2020.08.002.

1192 Zeron-Medina, J., Wang, X., Repapi, E., Campbell, M. R., Su, D., Castro-Giner, F., et al. (2013). A
1193 polymorphic p53 response element in KIT ligand influences cancer risk and has undergone
1194 natural selection. *Cell* 155, 410–22. doi: 10.1016/j.cell.2013.09.017.

1195 Zhan, Q., Bae, I., Kastan, M. B., and Fornace, A. J. (1994). The p53-dependent gamma-ray response of
1196 GADD45. *Cancer Res.* 54, 2755–2760.

1197 Zhan, Q., Chen, I.-T., Antinore, M. J., and Albert J. Fornace, J. (1998). Tumor Suppressor p53 Can
1198 Participate in Transcriptional Induction of the GADD45 Promoter in the Absence of Direct DNA
1199 Binding. *Mol. Cell. Biol.* 18, 2768. doi: 10.1128/mcb.18.5.2768.

1200 Zhang, S., Zhou, L., Hong, B., van den Heuvel, A. P. J., Prabhu, V. V., Warfel, N. A., et al. (2015).
1201 Small-Molecule NSC59984 Restores p53 Pathway Signaling and Antitumor Effects against
1202 Colorectal Cancer via p73 Activation and Degradation of Mutant p53. *Cancer Res.* 75, 3842–
1203 3852. doi: 10.1158/0008-5472.CAN-13-1079.

1204 Zhang, Y., and Dong, C. (2007). Regulatory mechanisms of mitogen-activated kinase signaling. *Cell.*
1205 *Mol. Life Sci.* 64, 2771–2789. doi: 10.1007/s00018-007-7012-3.

1206 Zhang, Y., Liu, T., Meyer, C. A., Eeckhoute, J., Johnson, D. S., Bernstein, B. E., et al. (2008). Model-
1207 based analysis of ChIP-Seq (MACS). *Genome Biol.* 9, R137. doi: 10.1186/gb-2008-9-9-r137.

1208 Zhu, J., Sammons, M. A., Donahue, G., Dou, Z., Vedadi, M., Getlik, M., et al. (2015). Gain-of-function
1209 p53 mutants co-opt chromatin pathways to drive cancer growth. *Nature* 525, 206–211. doi:
1210 10.1038/nature15251.

1211

FIGURE 1

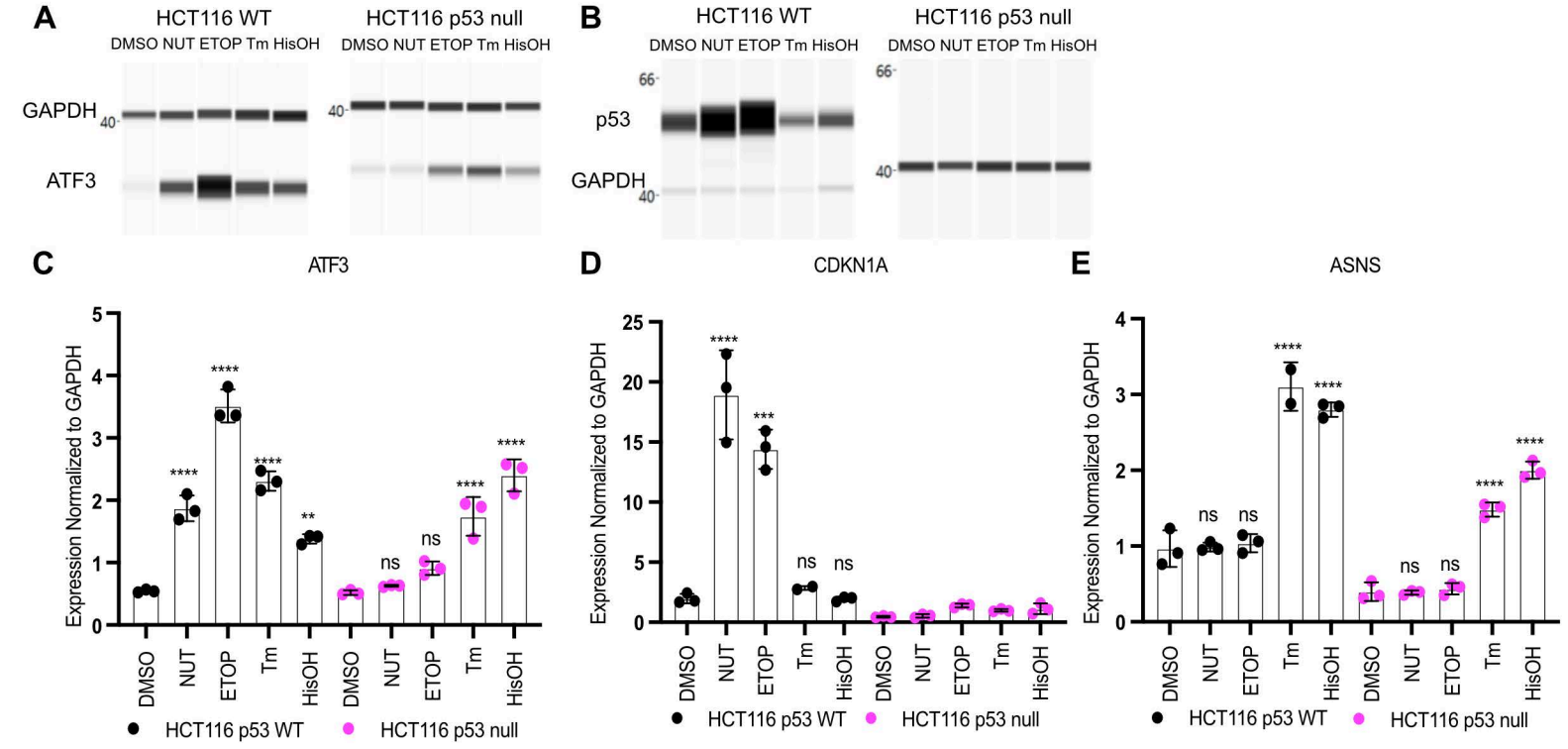
A
HCT116 WT
DMSO NUT ETOP Tm HisOH
HCT116 p53 null
DMSO NUT ETOP Tm HisOH
GAPDH
ATF3
40
B
HCT116 WT
DMSO NUT ETOP Tm HisOH
HCT116 p53 null
DMSO NUT ETOP Tm HisOH
66
p53
GAPDH
40
C
ATF3
D
CDKN1A
E
ASNS
Expression Normalized to GAPDH
DMSO
NUT
ETOP
Tm
HisOH
HCT116 p53 WT
HCT116 p53 null
****
***
**
ns

FIGURE 2

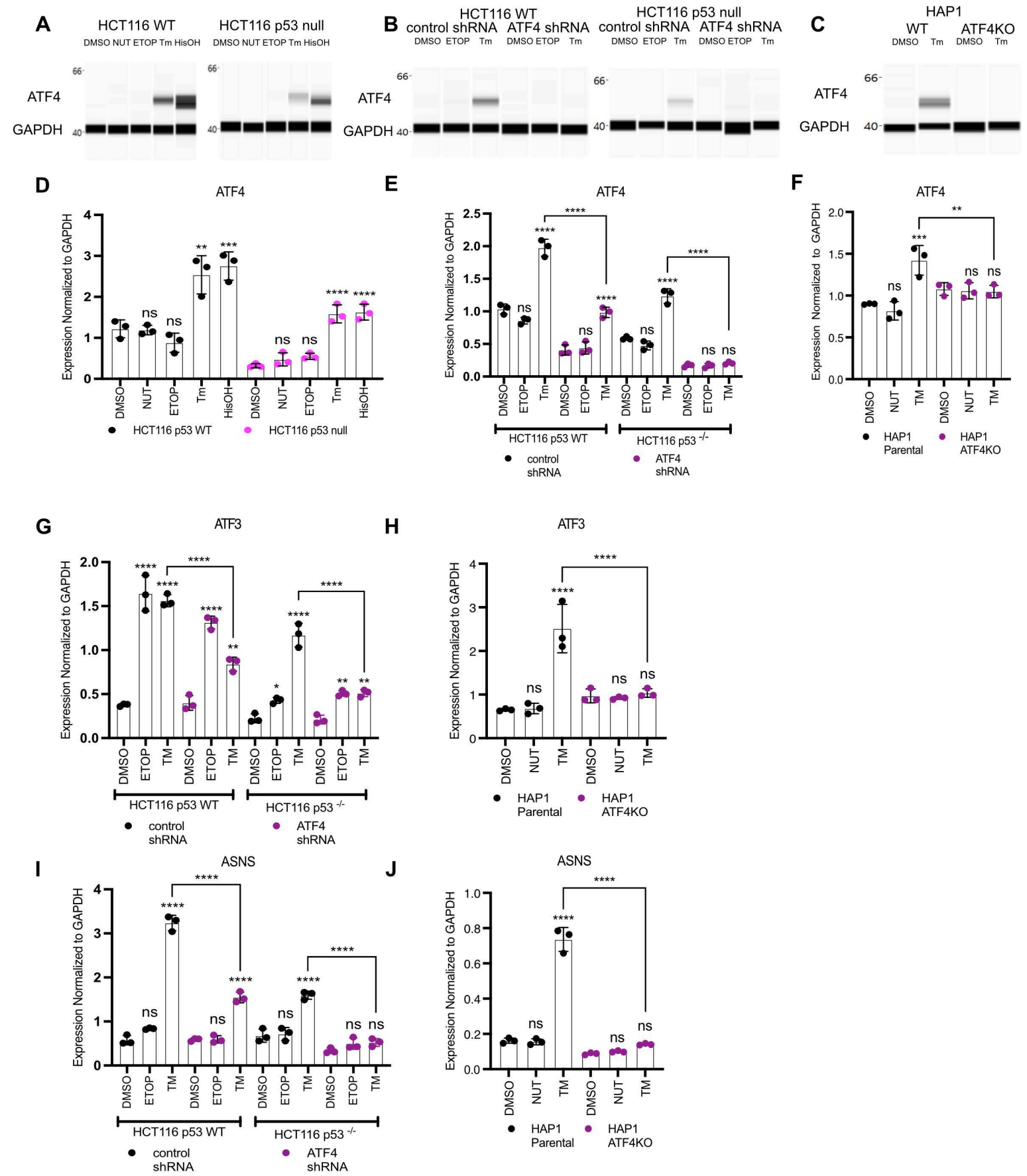
A
HCT116 WT
DMSO NUT ETOP Tm HisOH
HCT116 p53 null
DMSO NUT ETOP Tm HisOH
ATF4
GAPDH
B
HCT116 WT
control shRNA
ATF4 shRNA
HCT116 p53 null
control shRNA
ATF4 shRNA
C
HAP1
WT
ATF4KO
D
ATF4
Expression Normalized to GAPDH
HCT116 p53 WT
HCT116 p53 null
E
ATF4
HCT116 p53 WT
HCT116 p53 -/-
control shRNA
ATF4 shRNA
F
ATF4
HAP1 Parental
HAP1 ATF4KO
G
ATF3
HCT116 p53 WT
HCT116 p53 -/-
control shRNA
ATF4 shRNA
H
ATF3
HAP1 Parental
HAP1 ATF4KO
I
ASNS
HCT116 p53 WT
HCT116 p53 -/-
control shRNA
ATF4 shRNA
J
ASNS
HAP1 Parental
HAP1 ATF4KO

FIGURE 3

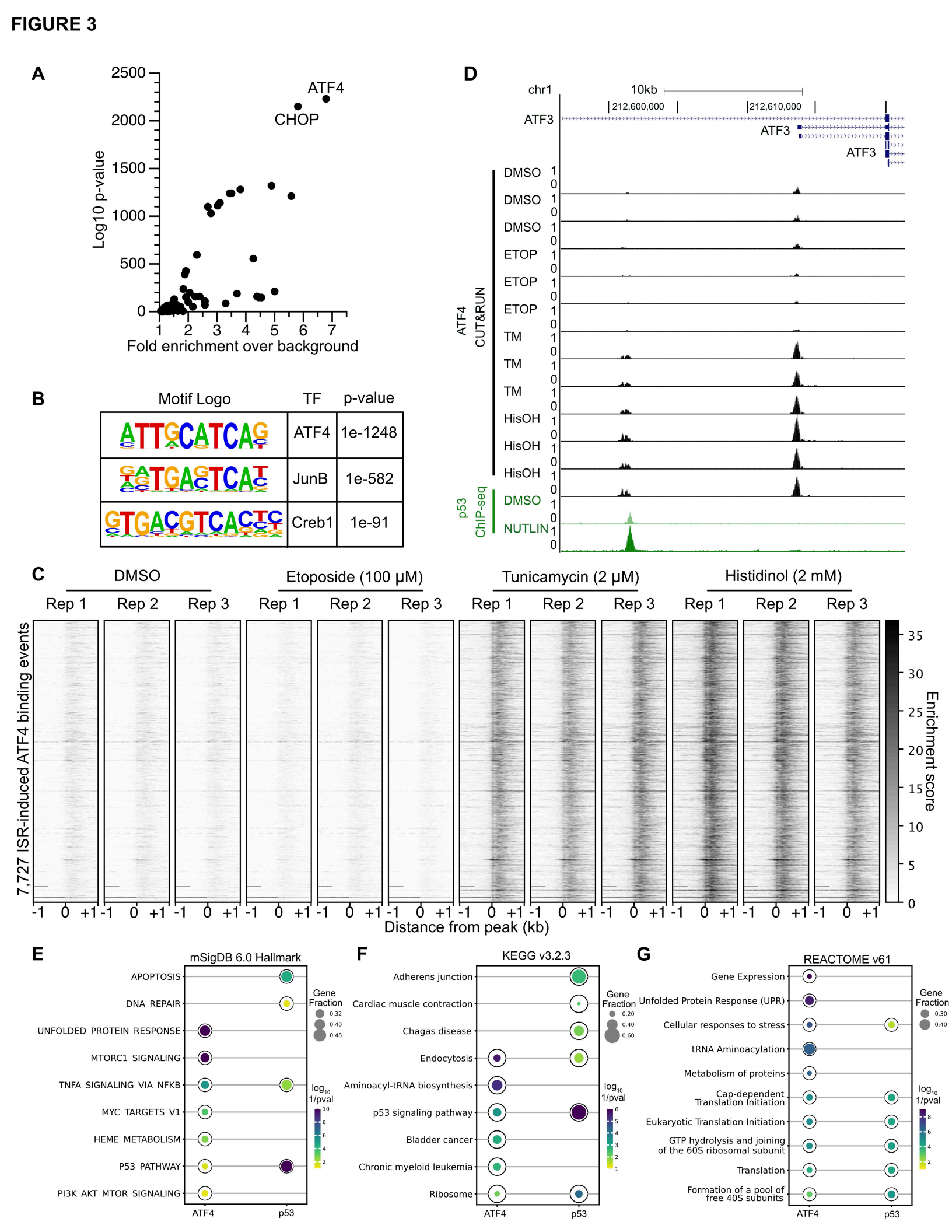
A
Log10 p-value
Fold enrichment over background
ATF4
CHOP
B
Motif Logo
TF
p-value
ATF4
1e-1248
JunB
1e-582
Creb1
1e-91
D
chr1
10kb
212,600,000
212,610,000
ATF3
ATF4 CUT&RUN
DMSO
ETOP
TM
HisOH
p53 ChIP-seq
NUTLIN
C
DMSO
Etoposide (100 μM)
Tunicamycin (2 μM)
Histidinol (2 mM)
Rep 1
Rep 2
Rep 3
7,727 ISR-induced ATF4 binding events
Enrichment score
Distance from peak (kb)
E
mSigDB 6.0 Hallmark
APOPTOSIS
DNA REPAIR
UNFOLDED PROTEIN RESPONSE
MTORC1 SIGNALING
TNFA SIGNALING VIA NFKB
MYC TARGETS V1
HEME METABOLISM
P53 PATHWAY
PI3K AKT MTOR SIGNALING
Gene Fraction
log10 1/pval
ATF4
p53
F
KEGG v3.2.3
Adherens junction
Cardiac muscle contraction
Chagas disease
Endocytosis
Aminoacyl-tRNA biosynthesis
p53 signaling pathway
Bladder cancer
Chronic myeloid leukemia
Ribosome
G
REACTOME v61
Gene Expression
Unfolded Protein Response (UPR)
Cellular responses to stress
tRNA Aminoacylation
Metabolism of proteins
Cap-dependent Translation Initiation
Eukaryotic Translation Initiation
GTP hydrolysis and joining of the 60S ribosomal subunit
Translation
Formation of a pool of free 40S subunits

FIGURE 4

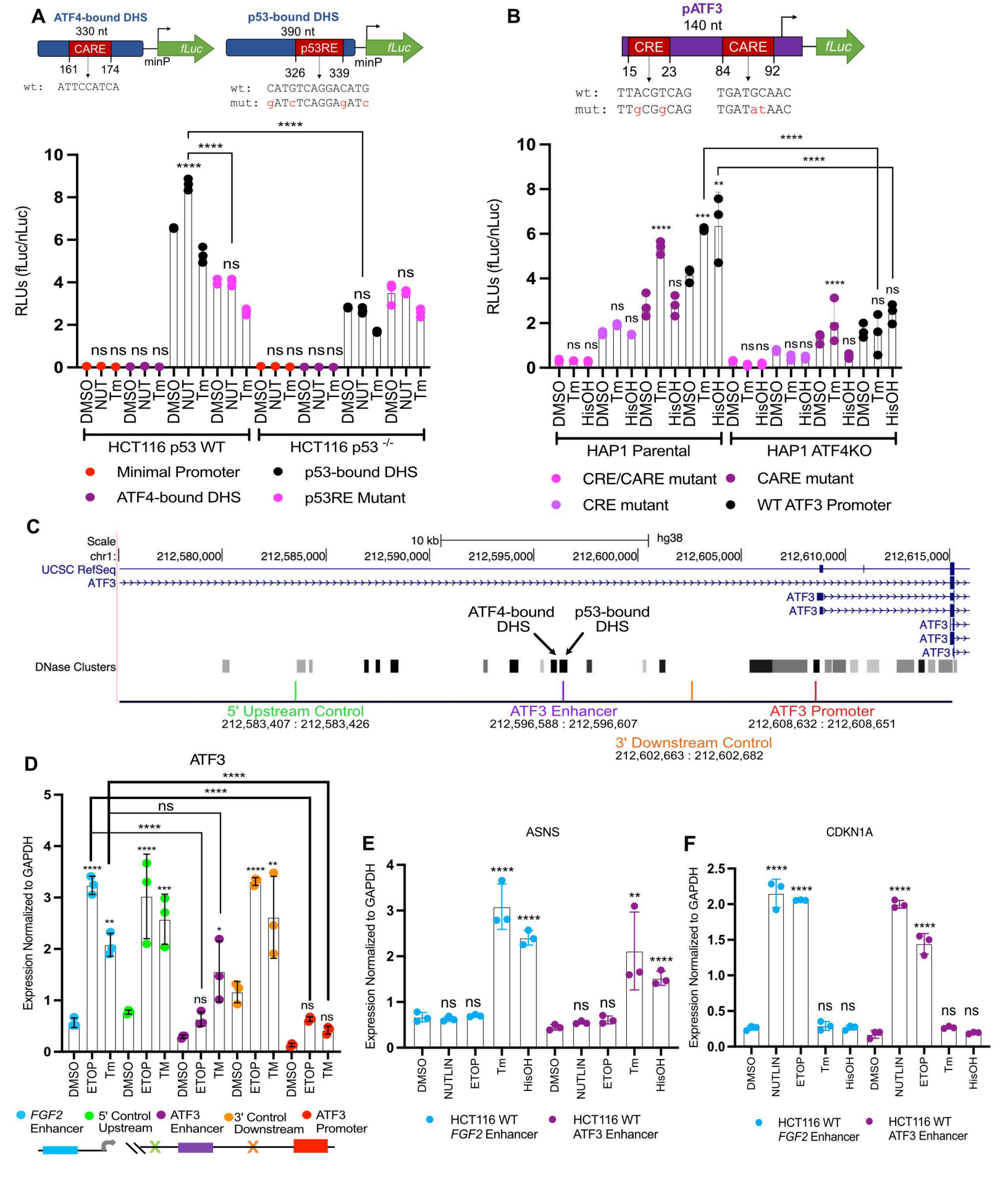
A
ATF4-bound DHS
330 nt
CARE
fLuc
minP
161
174
wt: ATTCCATCA
p53-bound DHS
390 nt
p53RE
326
339
wt: CATGTCAGGACATG
mut: gATcTCAGGAgATc
RLUs (fLuc/nLuc)
HCT116 p53 WT
HCT116 p53 -/-
Minimal Promoter
ATF4-bound DHS
p53-bound DHS
p53RE Mutant
B
pATF3
140 nt
CRE
CARE
15
23
84
92
wt: TTACGTCAG TGATGCAAC
mut: TTgCGgCAG TGATatAAC
HAP1 Parental
HAP1 ATF4KO
CRE/CARE mutant
CARE mutant
CRE mutant
WT ATF3 Promoter
C
Scale
chr1:
10 kb
hg38
UCSC RefSeq
ATF3
ATF4-bound DHS
p53-bound DHS
DNase Clusters
5' Upstream Control
212,583,407 : 212,583,426
ATF3 Enhancer
212,596,588 : 212,596,607
ATF3 Promoter
212,608,632 : 212,608,651
3' Downstream Control
212,602,663 : 212,602,682
D
ATF3
Expression Normalized to GAPDH
FGF2 Enhancer
5' Control Upstream
ATF3 Enhancer
3' Control Downstream
ATF3 Promoter
E
ASNS
HCT116 WT FGF2 Enhancer
HCT116 WT ATF3 Enhancer
F
CDKN1A
HCT116 WT FGF2 Enhancer
HCT116 WT ATF3 Enhancer

FIGURE 5

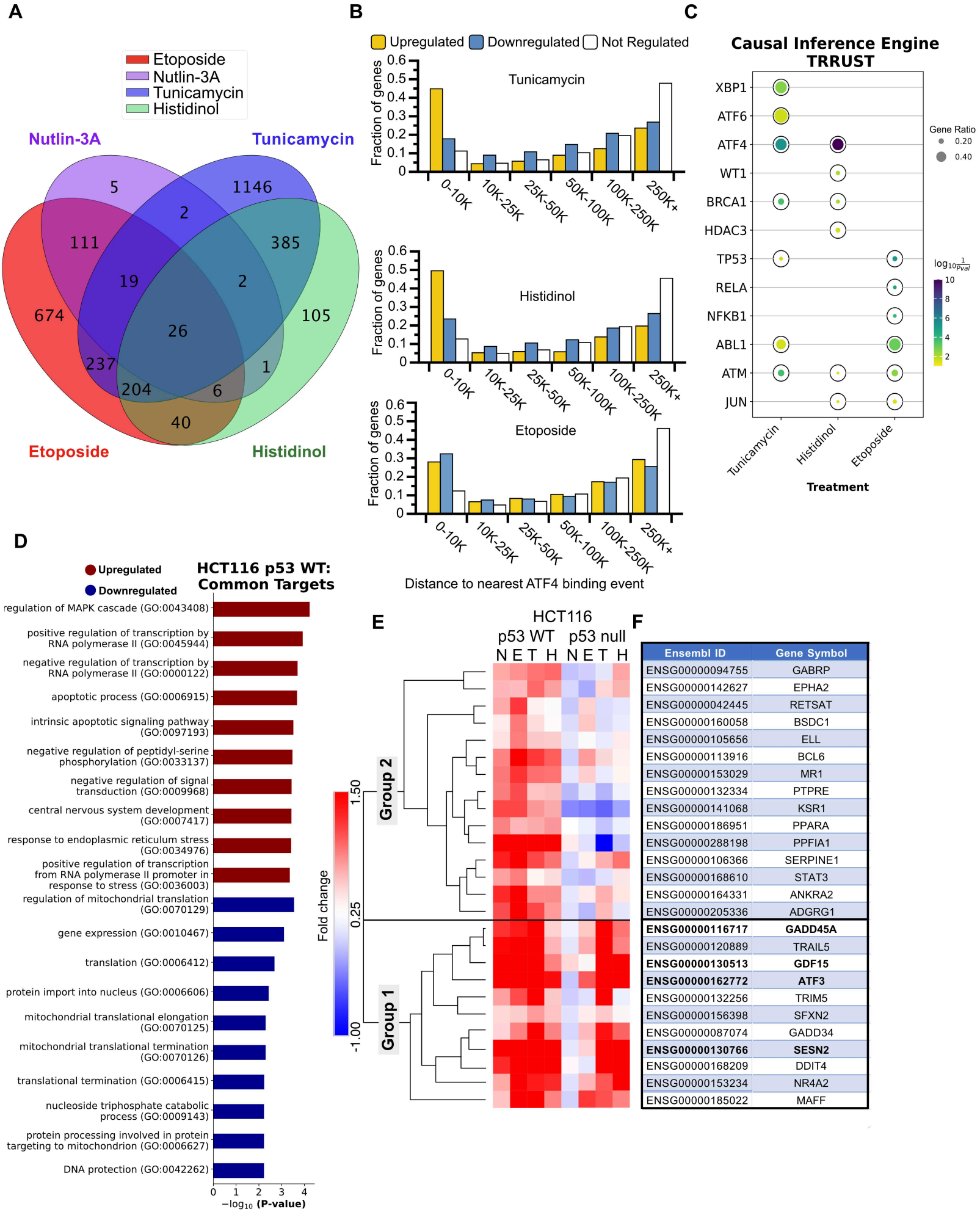

Ensembl ID	Gene Symbol
ENSG00000094755	GABRP
ENSG00000142627	EPHA2
ENSG00000042445	RETSAT
ENSG00000160058	BSDC1
ENSG00000105656	ELL
ENSG00000113916	BCL6
ENSG00000153029	MR1
ENSG00000132334	PTPRE
ENSG00000141068	KSR1
ENSG00000186951	PPARA
ENSG00000288198	PPFIA1
ENSG00000106366	SERPINE1
ENSG00000168610	STAT3
ENSG00000164331	ANKRA2
ENSG00000205336	ADGRG1
ENSG00000116717	**GADD45A**
ENSG00000120889	TRAIL5
ENSG00000130513	**GDF15**
ENSG00000162772	**ATF3**
ENSG00000132256	TRIM5
ENSG00000156398	SFXN2
ENSG00000087074	GADD34
ENSG00000130766	**SESN2**
ENSG00000168209	DDIT4
ENSG00000153234	NR4A2
ENSG00000185022	MAFF

FIGURE 6

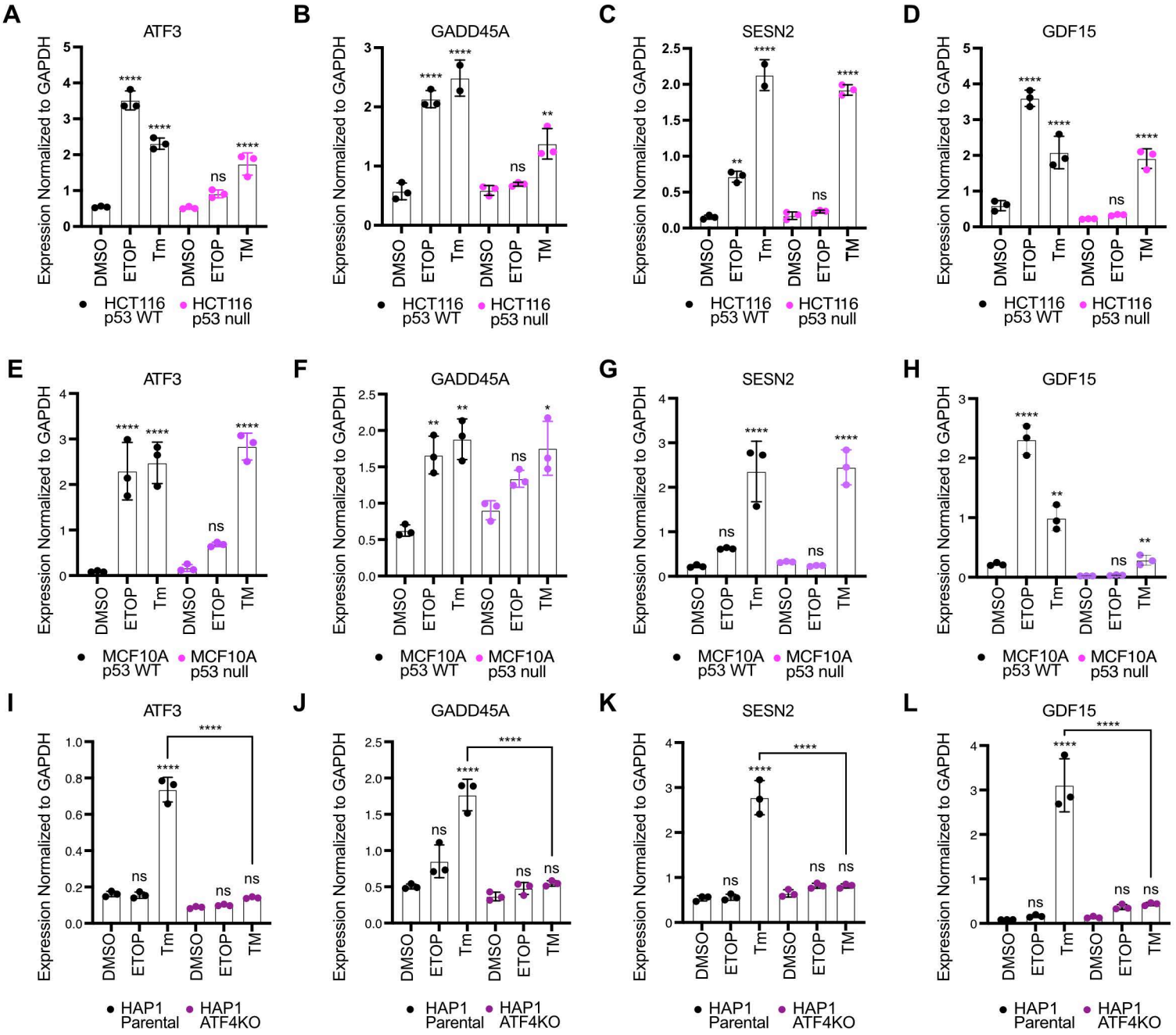
A
ATF3
B
GADD45A
C
SESN2
D
GDF15
E
ATF3
F
GADD45A
G
SESN2
H
GDF15
I
ATF3
J
GADD45A
K
SESN2
L
GDF15
Expression Normalized to GAPDH
DMSO
ETOP
Tm
DMSO
ETOP
TM
HCT116 p53 WT
HCT116 p53 null
MCF10A p53 WT
MCF10A p53 null
HAP1 Parental
HAP1 ATF4KO
****
**
*
ns

FIGURE 7

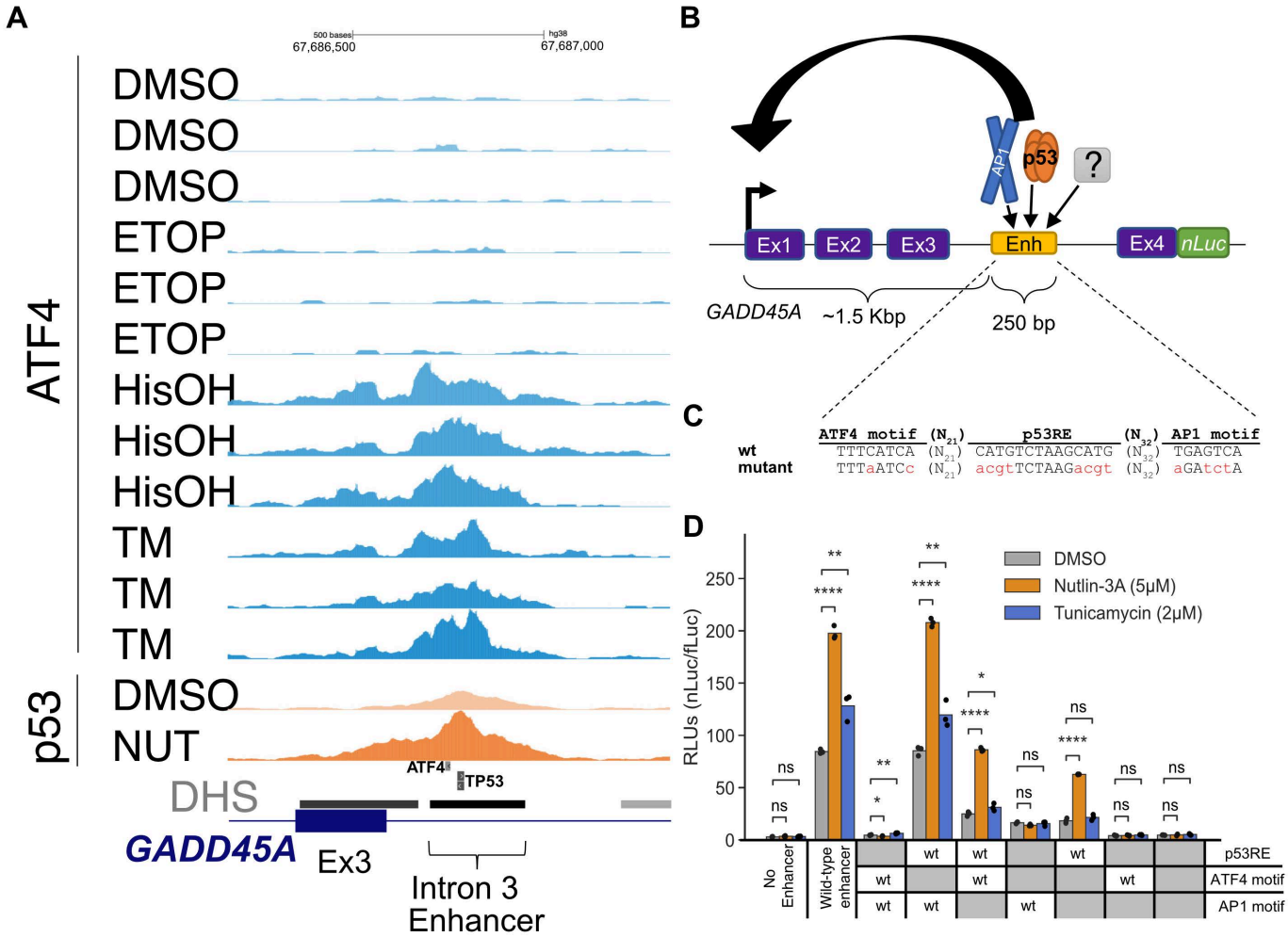
A
500 bases
hg38
67,686,500
67,687,000
ATF4
DMSO
DMSO
DMSO
ETOP
ETOP
ETOP
HisOH
HisOH
HisOH
TM
TM
TM
p53
DMSO
NUT
ATF4
TP53
DHS
GADD45A
Ex3
Intron 3
Enhancer
B
AP-1
p53
?
Ex1
Ex2
Ex3
Enh
Ex4
nLuc
GADD45A
~1.5 Kbp
250 bp
C
ATF4 motif (N21) p53RE (N32) AP1 motif
wt TTTCATCA (N21) CATGTCTAAGCATG (N32) TGAGTCA
mutant TTTaATCc (N21) acgtTCTAAGacgt (N32) aGAtctA
D
DMSO
Nutlin-3A (5μM)
Tunicamycin (2μM)
RLUs (nLuc/fLuc)
No Enhancer
Wild-type enhancer
p53RE
ATF4 motif
AP1 motif

FIGURE 8

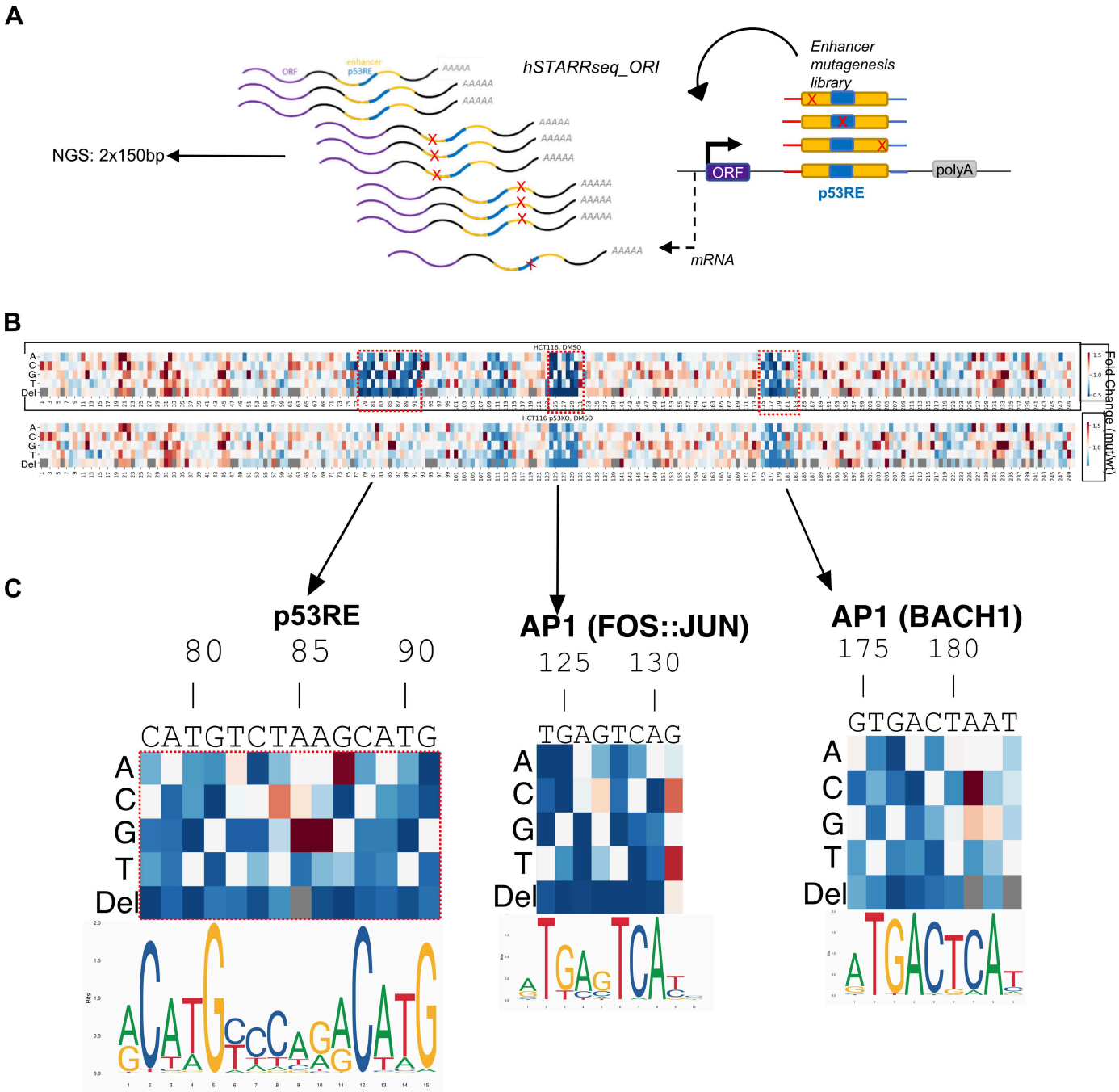
A
ORF
enhancer
p53RE
AAAAA
hSTARRseq_ORI
Enhancer mutagenesis library
NGS: 2x150bp
ORF
p53RE
polyA
mRNA
B
HCT116, DMSO
HCT116 p53KO, DMSO
A
C
G
T
Del
Fold Change (mut/wt)
C
p53RE
80
85
90
CATGTCTAAGCATG
AP1 (FOS::JUN)
125
130
TGAGTCAG
AP1 (BACH1)
175
180
GTGACTAAT
Bits

FIGURE 9

A

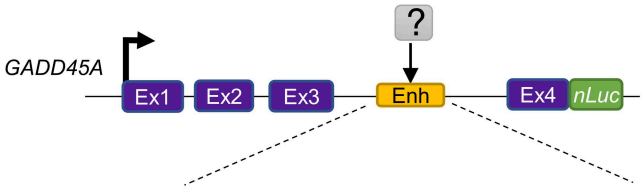

B

TF name	ETV6	AP1 (BACH1)	GLIS3/POU6F2
wt	AGCGGAAGAG (N_{58})	GTGACTAAT (N_{48})	CCCTCATTAAG
mut	AGCGGtgGAG (N_{58})	GTaACTcAT (N_{48})	CCgTCATaAAG
mut name	ETV6 (A112T) ETV6 (A113G)	BACH1 (G177A) BACH1 (A181C)	GLIS3 (C234G) POU6F2 (T239A)

C

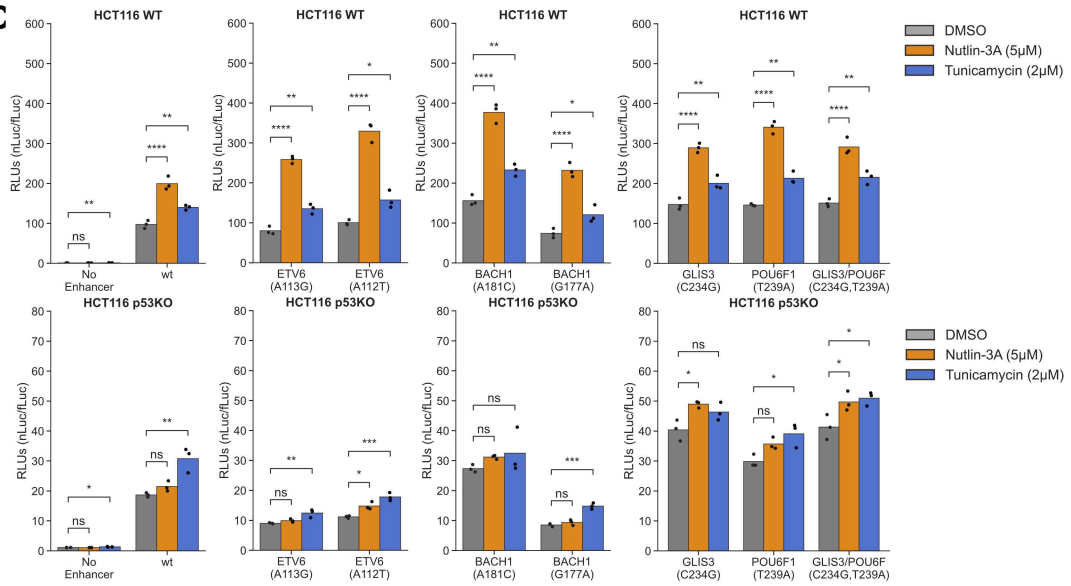

FIGURE S1

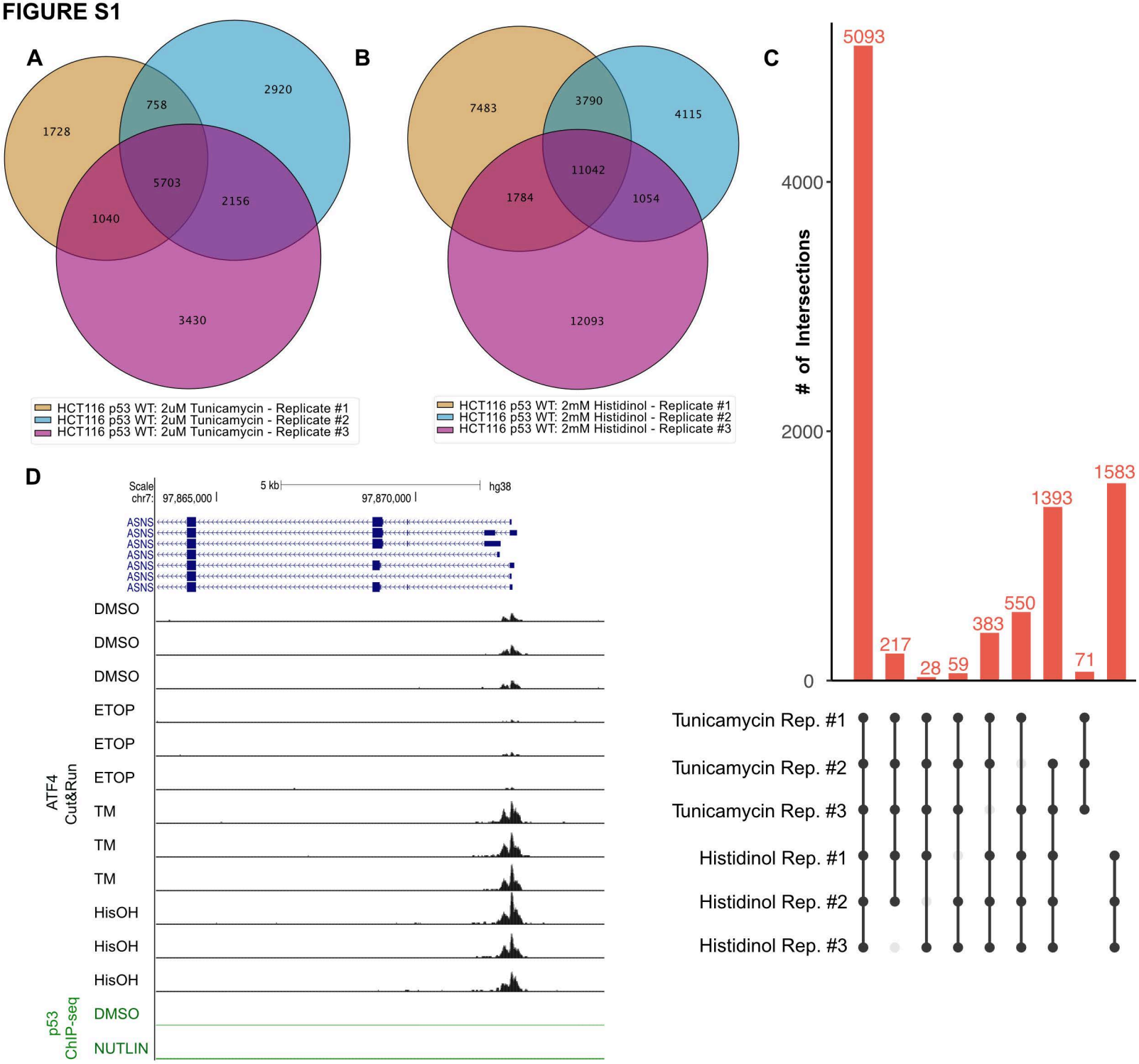
A
1728
758
2920
5703
1040
2156
3430
HCT116 p53 WT: 2uM Tunicamycin - Replicate #1
HCT116 p53 WT: 2uM Tunicamycin - Replicate #2
HCT116 p53 WT: 2uM Tunicamycin - Replicate #3
B
7483
3790
4115
11042
1784
1054
12093
HCT116 p53 WT: 2mM Histidinol - Replicate #1
HCT116 p53 WT: 2mM Histidinol - Replicate #2
HCT116 p53 WT: 2mM Histidinol - Replicate #3
C
# of Intersections
4000
2000
0
5093
217
28
59
383
550
1393
71
1583
Tunicamycin Rep. #1
Tunicamycin Rep. #2
Tunicamycin Rep. #3
Histidinol Rep. #1
Histidinol Rep. #2
Histidinol Rep. #3
D
Scale
chr7:
97,865,000
5 kb
97,870,000
hg38
ASNS
DMSO
ETOP
TM
HisOH
ATF4 Cut&Run
p53 ChIP-seq
NUTLIN

FIGURE S2

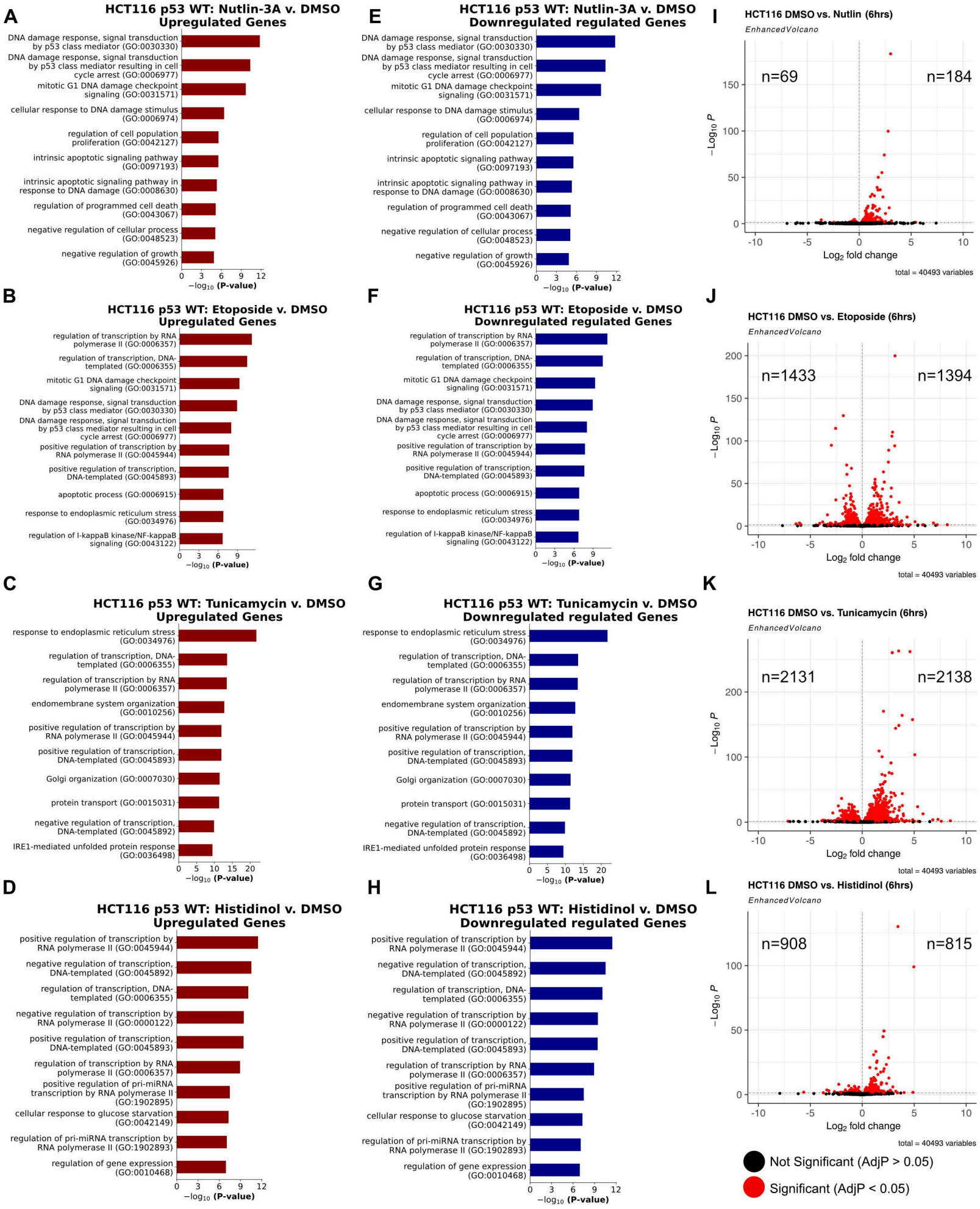
A
HCT116 p53 WT: Nutlin-3A v. DMSO
Upregulated Genes
DNA damage response, signal transduction by p53 class mediator (GO:0030330)
DNA damage response, signal transduction by p53 class mediator resulting in cell cycle arrest (GO:0006977)
mitotic G1 DNA damage checkpoint signaling (GO:0031571)
cellular response to DNA damage stimulus (GO:0006974)
regulation of cell population proliferation (GO:0042127)
intrinsic apoptotic signaling pathway (GO:0097193)
intrinsic apoptotic signaling pathway in response to DNA damage (GO:0008630)
regulation of programmed cell death (GO:0043067)
negative regulation of cellular process (GO:0048523)
negative regulation of growth (GO:0045926)
0 3 6 9 12
−log10 (P-value)
B
HCT116 p53 WT: Etoposide v. DMSO
Upregulated Genes
regulation of transcription by RNA polymerase II (GO:0006357)
regulation of transcription, DNA-templated (GO:0006355)
mitotic G1 DNA damage checkpoint signaling (GO:0031571)
DNA damage response, signal transduction by p53 class mediator (GO:0030330)
DNA damage response, signal transduction by p53 class mediator resulting in cell cycle arrest (GO:0006977)
positive regulation of transcription by RNA polymerase II (GO:0045944)
positive regulation of transcription, DNA-templated (GO:0045893)
apoptotic process (GO:0006915)
response to endoplasmic reticulum stress (GO:0034976)
regulation of I-kappaB kinase/NF-kappaB signaling (GO:0043122)
0 3 6 9
−log10 (P-value)
C
HCT116 p53 WT: Tunicamycin v. DMSO
Upregulated Genes
response to endoplasmic reticulum stress (GO:0034976)
regulation of transcription, DNA-templated (GO:0006355)
regulation of transcription by RNA polymerase II (GO:0006357)
endomembrane system organization (GO:0010256)
positive regulation of transcription by RNA polymerase II (GO:0045944)
positive regulation of transcription, DNA-templated (GO:0045893)
Golgi organization (GO:0007030)
protein transport (GO:0015031)
negative regulation of transcription, DNA-templated (GO:0045892)
IRE1-mediated unfolded protein response (GO:0036498)
0 5 10 15 20
−log10 (P-value)
D
HCT116 p53 WT: Histidinol v. DMSO
Upregulated Genes
positive regulation of transcription by RNA polymerase II (GO:0045944)
negative regulation of transcription, DNA-templated (GO:0045892)
regulation of transcription, DNA-templated (GO:0006355)
negative regulation of transcription by RNA polymerase II (GO:0000122)
positive regulation of transcription, DNA-templated (GO:0045893)
regulation of transcription by RNA polymerase II (GO:0006357)
positive regulation of pri-miRNA transcription by RNA polymerase II (GO:1902895)
cellular response to glucose starvation (GO:0042149)
regulation of pri-miRNA transcription by RNA polymerase II (GO:1902893)
regulation of gene expression (GO:0010468)
0 3 6 9 12
−log10 (P-value)
E
HCT116 p53 WT: Nutlin-3A v. DMSO
Downregulated regulated Genes
DNA damage response, signal transduction by p53 class mediator (GO:0030330)
DNA damage response, signal transduction by p53 class mediator resulting in cell cycle arrest (GO:0006977)
mitotic G1 DNA damage checkpoint signaling (GO:0031571)
cellular response to DNA damage stimulus (GO:0006974)
regulation of cell population proliferation (GO:0042127)
intrinsic apoptotic signaling pathway (GO:0097193)
intrinsic apoptotic signaling pathway in response to DNA damage (GO:0008630)
regulation of programmed cell death (GO:0043067)
negative regulation of cellular process (GO:0048523)
negative regulation of growth (GO:0045926)
0 3 6 9 12
−log10 (P-value)
F
HCT116 p53 WT: Etoposide v. DMSO
Downregulated regulated Genes
regulation of transcription by RNA polymerase II (GO:0006357)
regulation of transcription, DNA-templated (GO:0006355)
mitotic G1 DNA damage checkpoint signaling (GO:0031571)
DNA damage response, signal transduction by p53 class mediator (GO:0030330)
DNA damage response, signal transduction by p53 class mediator resulting in cell cycle arrest (GO:0006977)
positive regulation of transcription by RNA polymerase II (GO:0045944)
positive regulation of transcription, DNA-templated (GO:0045893)
apoptotic process (GO:0006915)
response to endoplasmic reticulum stress (GO:0034976)
regulation of I-kappaB kinase/NF-kappaB signaling (GO:0043122)
0 3 6 9
−log10 (P-value)
G
HCT116 p53 WT: Tunicamycin v. DMSO
Downregulated regulated Genes
response to endoplasmic reticulum stress (GO:0034976)
regulation of transcription, DNA-templated (GO:0006355)
regulation of transcription by RNA polymerase II (GO:0006357)
endomembrane system organization (GO:0010256)
positive regulation of transcription by RNA polymerase II (GO:0045944)
positive regulation of transcription, DNA-templated (GO:0045893)
Golgi organization (GO:0007030)
protein transport (GO:0015031)
negative regulation of transcription, DNA-templated (GO:0045892)
IRE1-mediated unfolded protein response (GO:0036498)
0 5 10 15 20
−log10 (P-value)
H
HCT116 p53 WT: Histidinol v. DMSO
Downregulated regulated Genes
positive regulation of transcription by RNA polymerase II (GO:0045944)
negative regulation of transcription, DNA-templated (GO:0045892)
regulation of transcription, DNA-templated (GO:0006355)
negative regulation of transcription by RNA polymerase II (GO:0000122)
positive regulation of transcription, DNA-templated (GO:0045893)
regulation of transcription by RNA polymerase II (GO:0006357)
positive regulation of pri-miRNA transcription by RNA polymerase II (GO:1902895)
cellular response to glucose starvation (GO:0042149)
regulation of pri-miRNA transcription by RNA polymerase II (GO:1902893)
regulation of gene expression (GO:0010468)
0 3 6 9 12
−log10 (P-value)
I
HCT116 DMSO vs. Nutlin (6hrs)
EnhancedVolcano
n=69
n=184
−Log10 P
Log2 fold change
total = 40493 variables
J
HCT116 DMSO vs. Etoposide (6hrs)
EnhancedVolcano
n=1433
n=1394
−Log10 P
Log2 fold change
total = 40493 variables
K
HCT116 DMSO vs. Tunicamycin (6hrs)
EnhancedVolcano
n=2131
n=2138
−Log10 P
Log2 fold change
total = 40493 variables
L
HCT116 DMSO vs. Histidinol (6hrs)
EnhancedVolcano
n=908
n=815
−Log10 P
Log2 fold change
total = 40493 variables
Not Significant (AdjP > 0.05)
Significant (AdjP < 0.05)

FIGURE S3

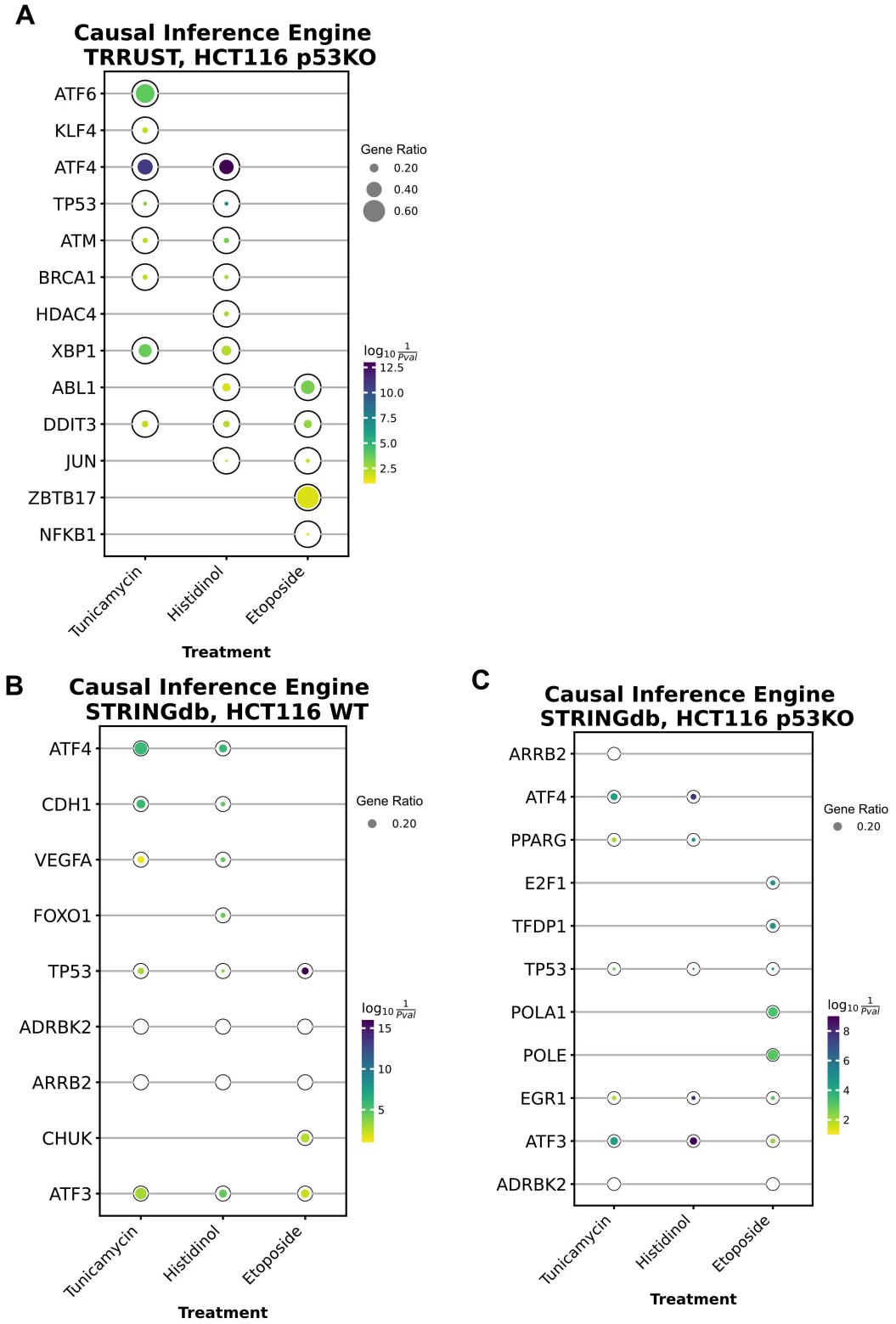
A
Causal Inference Engine
TRRUST, HCT116 p53KO
ATF6
KLF4
ATF4
TP53
ATM
BRCA1
HDAC4
XBP1
ABL1
DDIT3
JUN
ZBTB17
NFKB1
Tunicamycin
Histidinol
Etoposide
Treatment
Gene Ratio
0.20
0.40
0.60
$\log_{10}\frac{1}{Pval}$
12.5
10.0
7.5
5.0
2.5
B
Causal Inference Engine
STRINGdb, HCT116 WT
ATF4
CDH1
VEGFA
FOXO1
TP53
ADRBK2
ARRB2
CHUK
ATF3
Tunicamycin
Histidinol
Etoposide
Treatment
Gene Ratio
0.20
$\log_{10}\frac{1}{Pval}$
15
10
5
C
Causal Inference Engine
STRINGdb, HCT116 p53KO
ARRB2
ATF4
PPARG
E2F1
TFDP1
TP53
POLA1
POLE
EGR1
ATF3
ADRBK2
Tunicamycin
Histidinol
Etoposide
Treatment
Gene Ratio
0.20
$\log_{10}\frac{1}{Pval}$
8
6
4
2

FIGURE S4

A

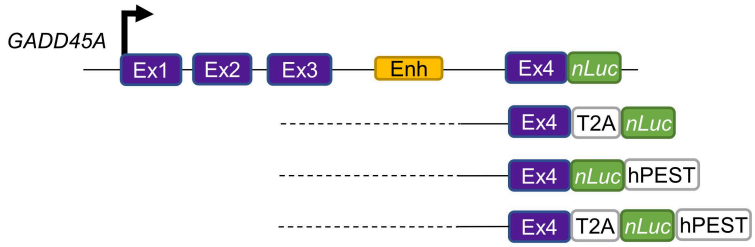
GADD45A
Ex1
Ex2
Ex3
Enh
Ex4
nLuc
Ex4
T2A
nLuc
Ex4
nLuc
hPEST
Ex4
T2A
nLuc
hPEST

B

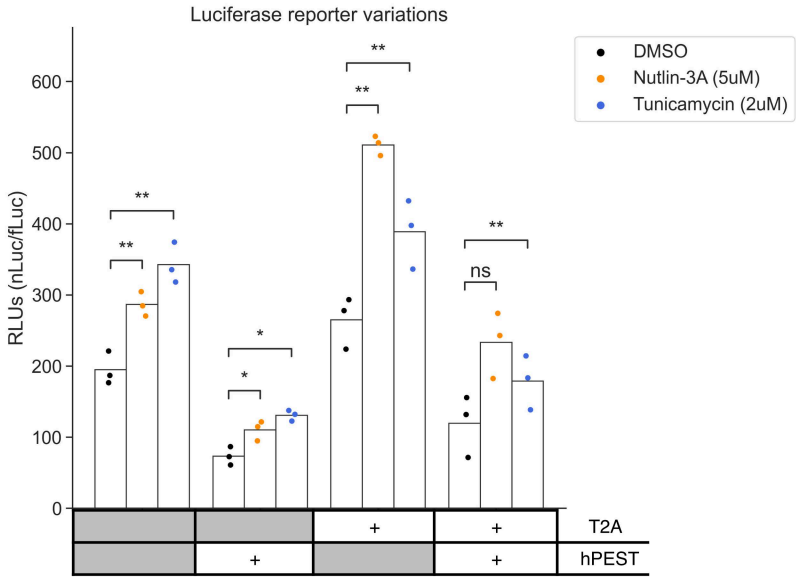
Luciferase reporter variations
RLUs (nLuc/fLuc)
0
100
200
300
400
500
600
DMSO
Nutlin-3A (5uM)
Tunicamycin (2uM)
**
**
*
*
**
**
**
ns
T2A
+
+
hPEST
+
+

FIGURE S5

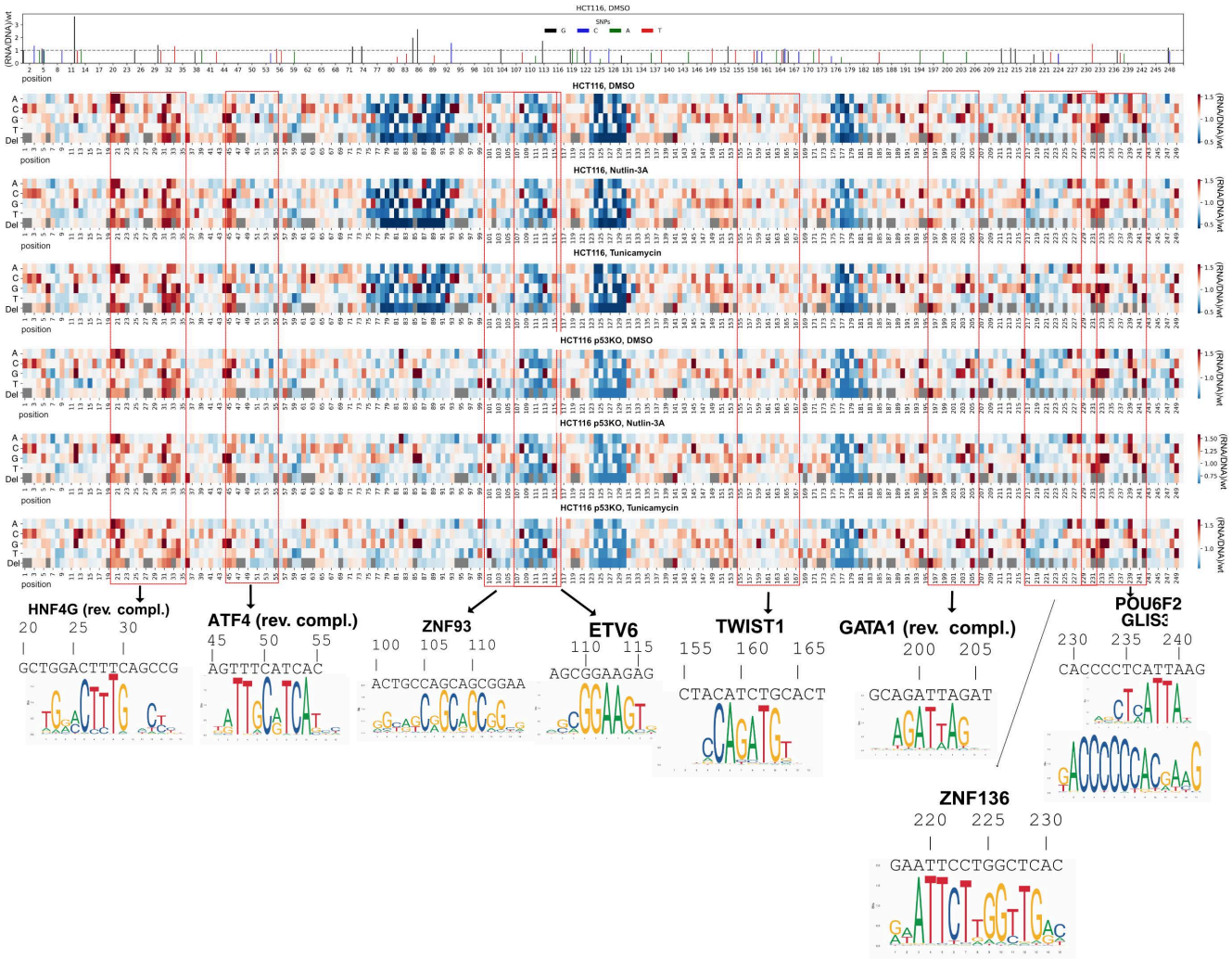
HCT116, DMSO
SNPs
G
C
A
T
(RNA/DNA)/wt
position
HCT116, DMSO
HCT116, Nutlin-3A
HCT116, Tunicamycin
HCT116 p53KO, DMSO
HCT116 p53KO, Nutlin-3A
HCT116 p53KO, Tunicamycin
A
C
G
T
Del
HNF4G (rev. compl.)
20 25 30
GCTGGACTTTCAGCCG
ATF4 (rev. compl.)
45 50 55
AGTTTCATCAC
ZNF93
100 105 110
ACTGCCAGCAGCGGAA
ETV6
110 115
AGCGGAAGAG
TWIST1
155 160 165
CTACATCTGCACT
GATA1 (rev. compl.)
200 205
GCAGATTAGAT
POU6F2
GLIS3
230 235 240
CACCCCTCATTAAG
ZNF136
220 225 230
GAATTCCTGGCTCAC